AMBIENT VIBRATION SIGNATURE ANALYSIS WITH SUBSPACE METHODS: CASE STUDIES

by

Bilge Alıcıoğlu

B.S., in C.E., Middle East Technical University, 2004

Submitted to the Institute for Graduate Studies in
Science and Engineering in partial fulfillment of
the requirements for the degree of
Master of Science

Graduate Program in Civil Engineering

Boğaziçi University

2006

AMBIENT VIBRATION SIGNATURE ANALYSIS WITH SUBSPACE METHODS: CASE STUDIES

APPROVED BY:

Assist. Prof. Hilmi Luş (Thesis Supervisor)	.....
Assoc. Prof. Osman S. Börekçi	.....
Assist. Prof. Sami A. Kılıç	.....

DATE OF APPROVAL: 09.06.2006

ACKNOWLEDGEMENTS

I would like to express my sincere gratitude to my thesis supervisor, Dr. Hilmi Luş. He has made this work possible in many ways, primarily by providing me a place in Boğaziçi University, and by offering excellent guidance and support during the course of this work. Without his understanding and friendly attitude, this study would not have been easy to handle.

I would also like to thank the members of my thesis committee, Dr. Osman S. Börekçi and Dr. Sami A. Kılıç, for their invaluable comments and suggestions.

I am also grateful to Dr. Sami F. Masri, University of Southern California, for providing the acceleration data from the Vincent Thomas Bridge; and Dr. Juan Caicedo, University of South Carolina, for both providing detailed information about the ASCE SHM benchmark problem and giving permission to use the photos on the website.

The economic support provided by the Turkish Scientific and Technical Research Council (TÜBİTAK) is greatly acknowledged.

I owe heartfelt gratitude to Dr. Engin Karaesmen and Dr. Erhan Karaesmen for their unchanging friendship, guidance and kind help during the last few years. Their sincere support has always encouraged and motivated me.

I am indebted to my officemates, Esra Mete Güneyisi, Cenk Güngör and Yavuz Tokmak, for their generous help and friendship during the last two years. Without them, my life in Bogaziçi would have never been the same.

Finally, I would like to thank my family and my dear friend, Onur Özer, for their great patience, support and love during this study.

ABSTRACT

AMBIENT VIBRATION SIGNATURE ANALYSIS WITH SUBSPACE METHODS: CASE STUDIES

This thesis addresses the issue of determining the structural modal parameters (natural frequencies, damping ratios and mode shapes) using the freely available ambient vibration measurements. The analysis methods considered for this purpose are the recently developed stochastic subspace identification algorithms that prove to be useful for ambient data analysis. These algorithms are essentially based on the assumption that the unmeasured excitation is the realization of a stochastic process, and try to fit state space models to the experimental data in the time domain. There are two different implementations of subspace methods. One of them converts the measured vibration signals to output covariances which can be considered as some sort of free decay response, and hence can be used to feed the realization algorithms originally formulated to treat impulse responses. The other algorithm, on the other hand, circumvents the covariance estimation step, and tries to fit a state space model directly on the raw output measurements by means of some projection techniques.

The first application in this study deals with the comparison of the two different identification algorithms with regards to their modal parameter identification capabilities. The comparison is handled by designing a Monte Carlo experiment based on the data simulated from a simple spring dashpot model. The relatively better performing algorithm is, then, used for the modal parameter identification of the IASC-ASCE structural health monitoring benchmark problem. The problem contains both an analytical and an experimental phase, and some implementation issues are discussed herein. The final case study concerns the modal analysis of the Vincent Thomas Suspension Bridge via the acceleration signals obtained under the operating conditions of the bridge.

ÖZET

ÇALIŞMA KOŞULLARI ALTINDA ELDE EDİLEN TİTREŞİM VERİLERİNİN ALTUZAY YÖNTEMLERİ İLE ÇÖZÜMLENMESİ: ÖRNEK İNCELEMELERİ

Bu çalışmada, bir yapıdan çalışma koşulları altında elde edilen titreşim verileri yardımıyla yapısal modal parametrelerin (özfrekanslar, sönüm oranları ve mod şekilleri) tespiti araştırılmıştır. Bu amaçla, yakın zamanlarda geliştirilen ve bu tür verilerin çözümlenmesinde faydalı olan olasılıksal altuzay sistem tanılama algoritmaları kullanılmıştır. Temelde, çalışma koşulları altında tespiti mümkün olmayan uyarımların rastgele bir süreç oldukları varsıyıma dayanan bu algoritmalar, deneysel verilere zaman bölgesinde durum uzay modelleri oturtmayı esas alırlar. Altuzay yöntemlerinin iki farklı şekilde uygulanması mümkündür. Bu uygulamalardan ilki, ölçülen titreşim sinyallerini ortak değişintilere çevirmek yoluyla bir çeşit serbest sönümlenme tepkisi hesaplar. Sonrasında, hesaplanan bu ortak değişintiler, esasen dürtü yanıtları ile çalışan gerçeklenebilirlik algoritmalarına girdi olarak kullanılırlar. İkinci uygulama ise ortak değişinti hesabını bir takım izdüşüm yöntemleri yardımıyla daha örtük bir şekilde hesaplayarak ham haldeki sinyaller üzerine bir durum uzay modeli oturtur.

Bu çalışmanın kapsamındaki ilk durum incelemesi, basit bir yay soğurucu siteminden benzetim kurularak elde edilen verilerin bir Monte Carlo deneyinde kullanılması ile ilgilir. Bu yolla, yukarıda sözü edilen iki farklı altuzay yönteminin modal parametre tanılamadaki yeterlikleri araştırılmıştır. Daha sonra, bu deneyde görece daha iyi performans gösteren yöntem, IASC-ASCE yapısal direnç kontrolü denektaşı problemine uygulanmıştır. Analitik ve deneysel olmak üzere iki ayrı fazdan oluşan bu problemin incelenmesi esnasında bazı uygulama sorunlarına temas edilmiştir. Çalışmadaki son durum incelemesi, Vincent Thomas Asma Köprüsü'nden çalışma koşulları altında elde edilmiş ivme ölçümlerinin köprünün modal anilizinde kullanılmasını içermektedir.

TABLE OF CONTENTS

LIST OF FIGURES

LIST OF TABLES

LIST OF SYMBOLS/ABBREVIATIONS

A	Discrete time state matrix
A_c	Continuous time state matrix
a_i	Real part of a complex number
B	Discrete time (first order) input matrix
B_c	Continuous time (first order) input matrix
B_f	Second order input matrix
b_i	Imaginary part of a complex number
C	Output matrix
$\tilde{c}_i$	Modal damping parameter
D	Direct transmission matrix
f_N	Nyquist frequency
f_s	Sampling frequency
G	State-output covariance matrix
H	Output data block Hankel matrix
I	Identity matrix
i	Half the number of block rows of the output data block Hankel matrix
J	Sum of the least squares residuals
j	Imaginary unit $j^2 = -1$
K	Stiffness matrix
k	Discrete time instant $t = k\Delta t,\ k \in \square$
$\tilde{k}_i$	Modal stiffness
l	Number of columns of the output data block Hankel matrix
M	Mass matrix
m	Number of outputs
$\tilde{m}_i$	Modal mass
N	Number of degree of freedoms in the spatial model
n	State space model order

O_i	Observability matrix with i block rows
$\underline{O}_i, \overline{O}_i$	Observability matrix with the last and first m rows truncated
P_i	Projection matrix of order i
$(P_i)_W$	Weighted projection matrix of order i
Q	Orthonormal matrix resulting from QR decomposition
$\widehat{Q}$	Process noise covariance matrix
$q(t)$	Displacement vector at time t
$\dot{q}(t)$	Velocity vector at time t
$\ddot{q}(t)$	Acceleration vector at time t
$\tilde{q}(t)$	Modal displacement vector at time t
$\dot{\tilde{q}}(t)$	Modal velocity vector at time t
$\ddot{\tilde{q}}(t)$	Modal acceleration vector at time t
R	Lower triangular matrix resulting from QR decomposition
R_i	Output covariance matrix at time lag i
$\widehat{R}$	Measurement noise covariance matrix
r	Number of inputs
r_i	Absolute value of a complex number
S	Diagonal matrix with positive singular values in descending order
$\widehat{S}$	Process-measurement noise covariance matrix
s	Number of time samples
T	Similarity transformation matrix
T_i	Block output covariance Toeplitz matrix of order i
$(T_i)_W$	Weighted block output covariances Toeplitz matrix of order i
t	Continuous time variable
Δt	Sampling interval
U	Left singular vectors
$u(k)$	Input vector at time instant k
$u(t)$	Input vector at time t
V	Right singular vectors

$v(k)$	Measurement noise vector at time instant k
W_1, W_2	Weighting matrices
$w(k)$	Process noise vector at time instant k
$\hat{X}_i$	Kalman filter state sequence
$x(k)$	State vector at time instant k
$x(t)$	State vector at time t
$\hat{x}(k)$	Kalman filter state estimate at time sample k
$\tilde{x}(t)$	Modal state vector at time t
$Y_f, Y_{i\|2i-1}$	Future output data block Hankel matrix
$Y_p, Y_{0\|i-1}$	Past output data block Hankel matrix
$Y_f^-, Y_{i+1\|2i-1}$	Future output data block Hankel matrix with the first block row deleted
$Y_p^+, Y_{0\|i}$	Past output data block Hankel matrix shifted one block row down
$y(k)$	Output vector at time instant k
$y(t)$	Output vector at time t
$z(t)$	Transformed state vector at time t
Δ_{MAC}	Allowable discrepancy for the correlation of two modal vectors
Δ_ω	Allowable distance between two natural frequency estimates
Δ_ζ	Allowable distance between two modal damping ratio estimates
δ	Coefficient of variation
δ_{pq}	Kronecker delta
$\varepsilon_w, \varepsilon_v$	Least squares residuals
Φ	Real eigenvector matrix of the spatial model
ϕ_i	Real eigenvectors (modal vectors) of the spatial model
Γ_i	Reversed stochastic controllability matrix with i block columns
Λ_c	Diagonal matrix containing the eigenvalues $\lambda_{c,i}$
Λ_d	Diagonal matrix containing the eigenvalues $\lambda_{d,i}$
$\lambda_{c,i}$	Complex eigenvalues of the continuous time state matrix A_c

$\lambda_{d,i}$	Complex eigenvalues of the discrete time state matrix A
λ_i	Complex eigenvalues of the spatial model
θ	An arbitrary angle
$\theta_{d,i}$	Phase angles of the complex eigenvalues $\lambda_{d,i}$
θ_i	Phase angle of a complex number
ρ_{MAC}	Allowable discrepancy for the correlation of two modal vectors
ρ_ω	Allowable discrepancy between two natural frequency estimates
ρ_ζ	Allowable discrepancy between two modal damping ratio estimates
Σ	State covariance matrix
τ	Threshold value for the distance between frequencies and damping ratios
Ω	Diagonal matrix containing the natural frequencies ω_i
ω_i	Undamped natural frequencies
Ξ	Damping matrix
Ψ	Complex eigenvector matrix
ψ	A complex modal vector
ψ_i	Complex eigenvectors of the state matrices A_c and A
$\bar{\psi}$	A complex modal vector rotated by an amount of θ rads
ζ_i	Modal damping ratio

ARMA	Auto Regressive Moving Average
ASCE	American Society of Civil Engineers
BR	Balanced Realization
CMIF	Complex Mode Indication Function
CVA	Canonical Variate Analysis
DOF	Degree of Freedom
ERA	Eigensystem Realization Algorithm
FE	Finite Element
IASC	International Association of Structural Control
MAC	Modal Amplitude Coherence
MPC	Modal Phase Collinearity

NExT	Natural Excitation Technique
N4SID	Numerical Algorithms for Subspace Identification
OKID	Observer/Kalman filter IDentification
PEM	Prediction Error Methods
PP	Peak Picking
PSD	Power Spectral Density
RD	Random Decrement
RMS	Root Mean Square
SHM	Structural Health Monitoring
SSI-COV	COVariance-Driven Stochastic Subspace Identification
SSI-DATA	DATA-driven Stochastic Subspace Identification
SVD	Singular Value Decomposition
ZOH	Zero Order Hold

1. INTRODUCTION

1.1. System Identification

In the broadest sense, a system can be described as an abstraction of reality, the time evolution of which can be described by a certain number of measurable attributes (Guidorzi, 2003). The most convenient way of representing a system is by means of mathematical models which can be viewed as sets of relations among those measurable attributes of a system. So by definition, the descriptive capability of mathematical models is restricted to the attributes that can be expressed by numbers, and therefore mathematical models provide only an approximation to the underlying true behavior. Despite this limitation, however, they have a major role in science and technology; consequently a need immediately arises for model construction procedures. These procedures can be classified into two general categories as physical modeling and system identification.

In physical modeling, the construction of a dynamic model is based on physical knowledge and the 'laws' governing the associated physical behavior. Since physical laws are, in turn, models deduced from observations, physical modeling is indeed constructing a model by means of some other abstractions of the reality. The advantage of physical modeling lies in the possibility of imposing a priori information on the system and using the physical meaning of the model variables.

Identification, on the other hand, consists of inferring a predefined type of mathematical model based on the observations performed on the system. Note that no restrictions are made in this brief description regarding the type of the initially assumed model, meaning that it may or may not have a direct physical interpretation. In the case where the selected model structure does not have a physical nature, the identified model is called a 'black box' model and the variables linked to it lack any physical meaning. Although black box modeling seems to be a crude way of describing a system, such models enjoy the advantage of being simple besides the capability of capturing only some relevant aspects from complex frameworks. Alternatively, the initially assumed model might be based on an a priori knowledge of the system's physical behavior, which in turn

is called a ‘white box’ model from an identification viewpoint. Thus, system identification should not be considered as a substitute of physical modeling, since it could be used together with models that have a physical origin in which case the identified variables correspond to the physical phenomena.

The broadness associated with the given description of system identification also explains the variety of applications it is used in. Some of these fields are medicine, economics, aerospace and civil engineering, to name just a few. The common feature of all the applications in these topics is that the behavior of the underlying dynamic system can be conceptually represented as an Input/Output model as sketched in Figure 1.1.

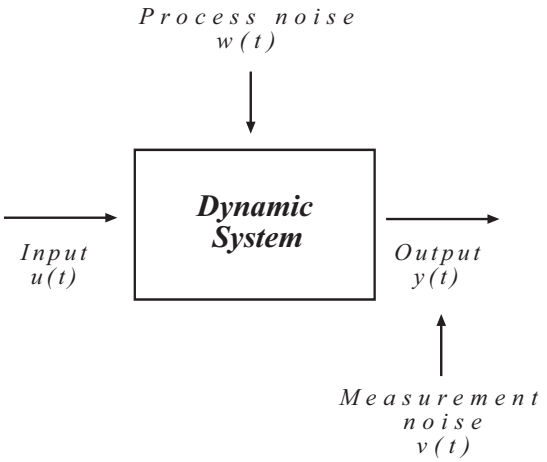

Figure 1.1. A conceptual description of a dynamic system

The system represented in Figure 1.1 is driven by the input $u(t)$ as well as some uncontrolled disturbance $w(t)$ called the ‘process noise’. The knowledge of $u(t)$ may or may not be available, but the term $w(t)$ remains totally unknown. The output $y(t)$ is the measured response of the system, and it usually is corrupted by some noise $v(t)$ due to observation inaccuracies.

The identification of such a dynamic system consists of three basic steps:

i. Collection of data: The purpose of identification is to replace the observed data $y(t)$ and $u(t)$ with a mathematical description of the mechanisms that generate it. So the

very initial step of the identification process is to collect the driving inputs and the corresponding system responses. (Note that in some cases, the collection of the input data may not be possible.)

ii. Selection of a model: A candidate model which is assumed to represent the internal system dynamics is chosen. The selection may rely upon a physical knowledge of the internal dynamics or simply on mathematical convenience.

iii. Computation of the model parameters: The parameter estimation step may be considered as an optimization problem in which the assumed model's variables are tuned according to the available observations.

1.2. System Identification in Civil Engineering

Structural systems have been the most fruitful research and application area of system identification in civil engineering. In this context, the system refers to a large scale structure such as a building, a bridge, or an offshore structure, while identification mostly involves the determination of the associated modal parameters (modal frequencies, damping ratios and mode shapes) of this structure.

The classical system identification algorithms have dealt with input-output mapping. This procedure involves the application of a measurable input to a system, measuring the corresponding response, and feeding these records altogether to the identification algorithm. The Prediction Error Methods (PEM) constitute one of the most traditional family of algorithms that cope with this kind of problem; see e.g. Ljung (1999). Two other families of algorithms are the realization based and direct subspace methods as classified by Viberg (1995). The realization based subspace algorithms require the impulse responses of a system which can be obtained either directly from impulse tests or inferred from any kind of forced response through some mathematical relations. These algorithms originate from the famous paper by Ho and Kalman (1966) in which the relationship between the impulse responses and the state space models has been established. The Eigensystem Realization Algorithm (ERA) proposed by Juang and Pappa (1985) is presumably the most notable realization based subspace algorithm, and it has been successfully implemented to several structures including the Galileo spacecraft (Pappa and Juang, 1985). The Observer/Kalman filter IDentification (OKID) recovers the system impulse responses from

the observer Markov parameters or Kalman filter derived from the experimental input-output data (Juang et al., 1993). The studies by Luş et al. (1999, 2002) constitute a successful integration of ERA/OKID for use in modal parameter identification and response prediction of civil structures. The direct subspace methods, on the other hand, are based on a rather implicit computation of these impulse responses by means of some projection techniques. The Numerical Algorithms for Subspace Identification (N4SID) proposed by Van Overschee and De Moor (1994) is arguably the most renowned algorithm of the direct subspace methods.

The difficulty concerning the application of these methodologies to civil structures is twofold. The first limitation is due to the impossibility of conducting experiments on the actual structures under controlled laboratory conditions. Consequently, the tests usually have to be performed in the field under operating conditions, and in this case the measurements of the dynamic forces are impossible. The application of artificial excitations under operating conditions might seem to be a solution, but besides the impracticality of exciting such large scale structures, there are so much uncontrolled disturbances that the thus acquired data is highly questionable. These concerns brought along the idea of using ambient vibrations measured under operational conditions which arise due to environmental factors such as wind and traffic. The more traditional approaches, in this context, are based on the analysis of ambient vibration signals in the frequency domain. Recently, some time domain identification algorithms that use only output data have also emerged. These algorithms assume that the unmeasured ambient excitations are realizations of a stationary stochastic process, and try to determine the desired model parameters on the basis of available response measurements. Although at a first glance this method might appear as an inferior alternative to the input-output identification algorithms, a study by Peeters et al. (2001a) has shown that ambient excitations indeed yield comparable results to the use of artificial excitation sources.

Most often, the assumed model structure for the identification of civil structures is a modal model consisting of modal frequencies, damping ratios and mode shapes. These notions will be elaborated in the following sections, so let it suffice to say, at this point of the discussion, that these parameters can completely characterize the dynamics of a vibrating structure. The simplest procedure for identifying the modal parameters using

ambient vibration responses only is perhaps the curve fitting techniques that work in frequency domain. Two of the most commonly used frequency domain identification techniques are the Peak Picking (PP) and the Complex Mode Indication Function (CMIF). The PP method is based on the selection of modal frequencies from the peaks of the spectrum plot of the output measurements as the name suggests. The analysis procedure can be found, for instance, in Bendat and Piersol (1980). The CMIF, on the other hand, diagonalizes the spectrum matrix, and tries to find the number of independent vibration modes in a more quantitative manner (Shih et al., 1988). A detailed review and comparison of these techniques can be found in Peeters (2000).

There also exist stochastic identification algorithms that work in time domain. One of these methods concerns fitting an Auto Regressive Moving Average (ARMA) model to the output data, and estimating the ARMA parameters using the PEM approach. This method has been successfully applied to civil structures (Andersen, 1997), but the highly nonlinear optimization problem involved in the parameter estimation step constitutes the main drawback for this procedure. Another notable example of these time domain algorithms is the Natural Excitation Technique (NExT) proposed by James et al. (1993). In this algorithm, the auto and cross correlation functions of output signals are treated as sums of decaying sinusoids which are considered to be similar to the free vibration response, and the modal parameters are extracted from these correlation functions. Along similar lines of reasoning, Ibrahim (1977) had proposed the Random Decrement technique (RD) which also converts the output signals to free decays using the RD functions. The other important group of stochastic identification algorithms, which is also the subject matter of the present study, is the subspace methods. Again the distinction will be made between the realization based and the direct subspace methods. The former algorithm is based on the solution of the stochastic realization problem (Akaike, 1974) and deals with obtaining the impulse responses by estimating the output covariances which can then be used in the realization algorithms. The direct method, on the other hand, circumvents the covariance estimation step by applying some projections on the output data (Van Overschee and De Moor, 1993).

In the field of civil engineering, system identification is inclined towards two major goals as classified by Franco (2003): Model calibration and vibration based structural health monitoring. The following sections include a brief overview of these applications.

1.2.1. Model Calibration

In civil engineering practice, it is customary to generate a physical idealization of the actual structure in the design process. Many approximations are made while creating this initial physical model. Besides, there might be some deviations from the structural and material properties specified in the design due to uncertainties involved in the construction process and time-dependent deterioration. Consequently, if this initial model is to be used for studying the behavior of the structure under operating conditions, it might be useful to update this model to account for such modeling inaccuracies and construction uncertainties. System identification provides a reliable way to fine tune the initial model based on experimental vibration measurements. Modal parameters are usually the most frequently identified structural parameters for this purpose (Ewins, 1995). A model updated in this manner has the capability of better reproducing the actual behavior of the structure, and hence is a more reliable tool to study the structure. A concise literature survey of existing model updating methods can be found in Mottershead and Friswell (1993).

1.2.2. Structural Health Monitoring

Structural health monitoring (SHM) is an active field of research which aims at obtaining qualitative and/or quantitative measures regarding the "health" condition of existing structures. According to the classification given by Rytter (1993), there exist four levels of damage identification:

i. Level 1 – Detection: Is any damage present in the structure or not?
ii. Level 2 – Localization: Where is the damage located within the structure?
iii. Level 3 – Assessment: What is the severity of damage?
iv. Level 4 – Prediction: What is the remaining service life of the structure?

The SHM methods can basically be classified as being local or global. Local methods concentrate on a part of a structure, and try to determine the damage within this specific part on the basis of experimental methods which include inducing acoustic waves,

eddy currents, X-rays, etc. In this perspective, these methods require a priori knowledge of the question in Level 2, and deal with Level 3 damage identification.

The global SHM methods, on the other hand, are generally based on vibration measurements obtained from the structure and are motivated from the fact that a local damage also affects the global response of the structure. In this context, the changes in modal parameters are usually considered as an implication of damage within the structure. Therefore, identification of modal parameters can be used as a Level 1 damage identification method. A concise overview of the existing damage detection techniques, which are based on the changes in modal parameter estimates, can be found in Farrar and Doebling (1997).

1.3. Scope and Outline

The present study focuses on two different identification algorithms that try to infer a model based on the ambient vibration measurements of a system. These algorithms are the COVariance-driven Stochastic Subspace Identification algorithm (SSI-COV), and the DATA-driven Stochastic Subspace Identification (SSI-DATA) as classified by Peeters and De Roeck (2001b). The initial issue concerns the comparative modal parameter identification capabilities of these methods. This will be discussed by means of simulating a very simple model. Following this analysis, one of these algorithms that have proven to be superior in the simulation step will be applied to two different structures: a four story steel frame and a long suspension bridge. The contents of the different sections in this thesis are given as follows:

In the second section of this study, three different mathematical representations of vibrating structures, namely the spatial, modal and state space models, are discussed, and the relations between them are shown. Next, the SSI-COV and SSI-DATA algorithms that identify state space models from response measurements are explained.

The third part involves the applications of subspace algorithms to several structures having different levels of complexities. The first example concerns a simple spring dashpot model, and this model is used for comparing the modal parameter identification

performances of the above mentioned algorithms. In the second application, a four story steel frame is considered. For this structure both an analytical and experimental model exist, so the application involves mainly two phases. The last structure in this study is a long suspension bridge.

The final section summarizes the conclusions of this study.

2. BASIC FORMULATIONS

2.1. Models of Vibrating Structures

2.1.1. Spatial and Modal Models

The continuous time equation of motion for a linear, time-invariant, N degree of freedom (DOF) model is given by

$$M\ddot{q}(t)+\Xi\dot{q}(t)+Kq(t)=B_f u(t) \tag{2.1}$$

In this second order differential equation, $M_{N\times N}$, $\Xi_{N\times N}$, and $K_{N\times N}$ are the mass, damping, and stiffness matrices, respectively, of dimensions $N\times N$. The vector $q(t)$, of dimensions $N\times 1$, contains the displacements associated with all the DOFs at continuous time t, and overdots designate differentiation with respect to time with $\dot{q}(t)$ representing the velocity and $\ddot{q}(t)$ the acceleration vector. The force vector $u(t)$ describes the r inputs applied at time t, and the second order input matrix B_f, of dimensions $N\times r$, maps these inputs to their corresponding point(s) of application on the system.

The model described in Eq. (2.1) is called the spatial model since it describes the system by means of its physical and geometrical characteristics such as the distribution of mass, rigidity, and damping. For civil engineering structures which have distributed mass and stiffness properties, Eq. (2.1) can be obtained as the N DOF Finite Element (FE) approximation of the system. In this approach, the structure would be divided into elements, and the mass and stiffness matrices would be constructed by means of the geometry and material properties of these elements. As for the damping properties, viscous damping assumption is generally used to reproduce the observed decaying motions of vibrating structures. The largest uncertainty in this model can be said to be associated with the damping matrix due to a lack of precise knowledge of damping mechanisms in civil structures.

The N equations implicitly involved in Eq. (2.1) are coupled, and need to be solved simultaneously. It is possible, on the other hand, to uncouple these equations, and rewrite them in N independent coordinates. Each of these coordinates can then be considered as an independent vibration mode characterized by a frequency, damping ratio and mode shape. The resulting model in this case is called a modal model, and describes the way in which a system vibrates naturally, e.g. without any externally applied force.

In order to obtain the modal model by means of the spatial model, consider first the solution to the homogenous spatial model without damping:

$$M\ddot{q}(t) + Kq(t) = 0 \tag{2.2}$$

The solution is assumed to have the following form: $q(t) = \phi_i e^{j\omega_i t}$ where j is the imaginary unit defined as $j^2 = -1$, and $i = 1, 2..., N$ (the range for i will be the same for the rest of the discussion in Section 2.1). By inserting this solution into Eq. (2.2) an eigenvalue problem is obtained such that

$$(K - \omega_i^2 M)\phi_i = 0 \tag{2.3}$$

where ω_i and ϕ_i are the i^{th} (real) eigenvalue and eigenvector, respectively. All N eigenvalue problems given in Eq. (2.3) can be combined in a single matrix expression as

$$K\Phi = M\Phi\Omega^2 \tag{2.4}$$

where $\Phi_{N\times N}$ contains the eigenvectors ϕ_i as columns, and $\Omega_{N\times N}$ is a diagonal matrix with the corresponding eigenvalues ω_i as its nonzero entries. It can be shown that the following orthogonality conditions hold true

$$\Phi^T M\Phi = diag\left(\tilde{m}_i\right), \quad \Phi^T K\Phi = diag\left(\tilde{k}_i\right) \tag{2.5}$$

where $\tilde{m}_i$ and $\tilde{k}_i$ are defined as the modal masses and stiffnesses, $diag(\bullet)$ symbolizes a diagonal matrix whose nonzero elements are those specified inside the brackets, and $(\bullet)^T$ denotes matrix transpose. Introducing Eq. (2.5) into Eq. (2.4) yields

$$\omega_i^2 = \frac{\tilde{k}_i}{\tilde{m}_i} \tag{2.6}$$

and this leads to the conclusion that the eigenvalues ω_i are the undamped natural frequencies (in rad/s) as defined in structural vibrations. The eigenvectors also correspond to the so-called mode shapes which define the deformed shape of a structure vibrating at its natural frequency.

It is very important to realize at this stage that the eigenvalue matrix Ω is unique, whereas the eigenvector matrix Φ is not. Even though the natural frequencies are fixed quantities, the mode shapes can be scaled arbitrarily without changing the shape of the vibration mode while changing its amplitude. Among the many possible scaling choices, the most commonly preferred one is the mass normalization which in turn allows rewriting Eq. (2.5) as

$$\Phi^T M \Phi = I_{N\times N}, \quad \Phi^T K \Phi = \Omega^2 \tag{2.7}$$

where $I_{N\times N}$ is an identity matrix.

If the eigenvector matrix Φ also diagonalizes the damping matrix such that

$$\Phi^T \Xi \Phi = diag(\tilde{c}_i) = diag(2\zeta_i \omega_i \tilde{m}_i) = diag(2\zeta_i \omega_i)\, diag(\tilde{m}_i) \tag{2.8}$$

where ζ_i are the modal damping ratios defined as $\zeta_i = \tilde{c}_i / 2\tilde{m}_i\omega_i$, the spatial model given in Eq (2.1) can completely be split into independent modal coordinates. Introducing the transformation $\tilde{q}(t) = \Phi q(t)$, and making use of Eq. (2.7) and (2.8); Eq. (2.1) can be rewritten as follows:

$$\ddot{\tilde{q}}(t) + diag\left(2\zeta_i\omega_i\right)\dot{\tilde{q}}(t) + \Omega^2\tilde{q}(t) = diag\left(1/\tilde{m}_i\right)\Phi^T B_f u(t) \tag{2.9}$$

Here $\tilde{q}(t)$ contains the N modal displacements at continuous time. If the solution to the homogenous part of Eq. (2.9) is assumed to have the form $\tilde{q}(t) = \phi_i e^{\lambda_i t}$, this leads to the following the eigenvalue problem:

$$(\lambda_i^2 + 2\zeta_i\omega_i\lambda_i + \omega_i^2)\phi_i = 0 \tag{2.10}$$

Owing to the assumption made in Eq. (2.8), the eigenvectors are the same as in the undamped case. Provided that the system is underdamped, i.e. $\zeta_i < 1$, the eigenvalues will be given by

$$\lambda_i, \lambda_i^* = -\zeta_i\omega_i \pm j\omega_i\sqrt{1-\zeta_i^2} \tag{2.11}$$

where $(\bullet)^*$ denotes complex conjugate. In this case, the undamped natural frequencies and modal damping ratios can be extracted from Eq. (2.11) as

$$\begin{aligned} \omega_i &= \sqrt{\mathrm{Re}\left(\lambda_i\right)^2 + \mathrm{Im}\left(\lambda_i\right)^2} \\ \zeta_i &= \frac{-\mathrm{Re}\left(\lambda_i\right)}{\omega_i} = \frac{-\mathrm{Re}\left(\lambda_i^*\right)}{\omega_i} \end{aligned} \tag{2.12}$$

where $\mathrm{Re}(\bullet)$ and $\mathrm{Im}(\bullet)$ represent the real and imaginary parts of a complex number. A system that can be reduced to the form in Eq. (2.9) is said to be classically damped. If a damping description is ever needed in a FE modeling process, it is customary to assign modal damping ratios to the modes of interest. These values might, for instance, be obtained from an experimental modal analysis.

Although classical damping assumption is often used in theoretical analysis of structures, it is valid for a very special distribution of damping which may not generally apply to the real structures. The general viscous damping assumption, on the other hand,

covers both the classical as well as the non-classical damping cases. In the latter case, the eigenvector matrix of the solution to the homogenous undamped equation of motion does not diagonalize the damping matrix, so the assumption introduced in Eq. (2.8) is not valid anymore.

In the general viscous damping case, a solution of the form $\tilde{q}(t) = \psi_i e^{\lambda_i t}$ can be assumed for the homogenous part of Eq. (2.1), and this yields the following eigenvalue problem:

$$\left(\lambda_i^2 M + \lambda_i \Xi + K\right)\psi_i = 0 \tag{2.13}$$

Note that in Eq. (2.13) the eigenvectors ψ_i are represented with a different notation. This is because they appear in complex conjugate pairs (i.e., ψ_i, ψ_i^*) as opposed to the real eigenvectors in the classical damping case. An efficient way to solve this problem is to transform it to a symmetric generalized eigenvalue problem. For this purpose, the second order spatial model should be converted into a first order representation. The solution will not be presented in the context of this discussion, but detailed derivations concerning the solution of this eigenvalue problem can be found, for instance, in Luş et al. (2003). The non-classical damping case is mentioned here briefly in order to enable a better understanding of the link between the state space models of the following section and the modal models described herein. Throughout this study, however, classical damping assumption will be imposed on the identified modal models.

2.1.2. State Space Models

Although Eq. (2.1) provides an accurate representation of a system, constructing such a second order spatial model is not the primary concern in this study. The model given in Eq. (2.1) will rather be used as a starting point to show the relationship of state space models to the second order formulation. By introducing the following vector and matrix definitions

$$x(t)=\begin{Bmatrix} q(t) \\ \dot{q}(t) \end{Bmatrix},\ A_c=\begin{bmatrix} 0_{N\times N} & I_{N\times N} \\ -M^{-1}K & -M^{-1}\Xi \end{bmatrix},\ B_c=\begin{bmatrix} 0_{N\times N} \\ M^{-1}B_f \end{bmatrix} \tag{2.14}$$

where $0_{N\times N}$ is an $N\times N$ matrix full of zeros, Eq. (2.1) can be cast into the first order form in which the system dynamics are described by

$$\dot{x}(t)=A_c x(t)+B_c u(t) \tag{2.15}$$

Eq. (2.15) is referred to as the continuous time state equation. Here, $x(t)$ is the n ($n=2N$) dimensional state vector that contains the displacements and velocities at time t. A_c is the $n\times n$ continuous time state matrix which characterizes all the system dynamics such as mass, damping and stiffness properties (hence the modal parameters), and B_c is the $n\times r$ continuous time (first order) input matrix that describes how the input term influences the state. (The subscript c is to denote continuous from hereafter). Note that the order of the state matrix n is equal to two times the number of vibration modes, and will be referred to as the system order from here onwards.

In experimental vibration problems, it is simply impossible to measure all DOFs that are specified in the spatial modal. This is also not necessary since the number of measurements that is sufficient to accurately determine the modal parameters is some orders of magnitude smaller than the DOFs needed for an accurate spatial model. Consequently, an additional equation that interconnects the internal state and the observed output measurements is needed. An output vector $y(t)$ is defined for this purpose, and it can be related to the state vector (and the input vector if the measurements involve acceleration readings) through

$$y(t)=Cx(t)+Du(t) \tag{2.16}$$

where $y(t)$ is an $m\times 1$ vector containing the response measurements at time t. C is the $m\times n$ output matrix that maps the internal states to the observed signals, and can be constructed as a subset of the rows of the matrix

$$\begin{bmatrix} I_{N\times N} & 0_{N\times N} \\ 0_{N\times N} & I_{N\times N} \\ -M^{-1}K & -M^{-1}\Xi \end{bmatrix} \tag{2.17}$$

depending on whether displacements, velocities and/or accelerations are measured at a DOF. Finally, D is the direct transmission matrix which describes the direct effect of the input term on the output measurements without the need to go through the intermediary state equation. It has dimensions $m\times r$ and is nonzero only if measurements contain acceleration readings. Similarly, the rows of D are selected from the rows of the matrix $\left[M^{-1}B_f\right]$.

The complete continuous time state space representation of the linear, time invariant system is given by the combination of Eqs. (2.15) and (2.16):

$$\begin{aligned} \dot{x}(t) &= A_c x(t) + B_c u(t) \\ y(t) &= Cx(t) + Du(t) \end{aligned} \tag{2.18}$$

It is possible to define a new state vector by considering the transformation

$$x(t) = Tz(t) \tag{2.19}$$

where $T_{n\times n}$ is a nonsingular matrix. By introducing this coordinate transformation into Eq.(2.18), the state space model can be rewritten as

$$\begin{aligned} \dot{z}(t) &= T^{-1}A_c Tz(t) + T^{-1}B_c u(t) \\ y(t) &= CTz(t) + Du(t) \end{aligned} \tag{2.20}$$

The most important implication of Eq. (2.20) is that it describes exactly the same input-output mapping as Eq. (2.18), and for this reason Eq. (2.19) is said to be a similarity transformation. Note, however, that the new state vector $z(t)$ does not contain the displacements and velocities expressed in spatial coordinates anymore.

This transformation property can also be employed to establish the relations between a state space model and a modal model. Consider, for this purpose, the eigenvalue decomposition of the continuous time state matrix given by

$$A_c = \Psi \Lambda_c \Psi^{-1} \tag{2.21}$$

where Λ_c is a diagonal matrix with the n complex eigenvalues (that appear in complex conjugate pairs $\lambda_{c,i}, \lambda_{c,i}^*$ if all modes are underdamped) as its nonzero entries, and $\Psi_{n \times n}$ contains the corresponding complex eigenvector pairs ψ_i, ψ_i^* of A_c. If the complex modal states are denoted by $\tilde{x}(t)$, then $x(t) = \Psi \tilde{x}(t)$ represents a special similarity transformation (where $T = \Psi$) which when introduced into Eq. (2.18) yields the modal state space model as

$$\begin{aligned} \dot{\tilde{x}}(t) &= \Lambda_c \tilde{x}(t) + \Psi^{-1} B_c u(t) \\ y(t) &= C \Psi \tilde{x}(t) + D u(t) \end{aligned} \tag{2.22}$$

In the special case of classical damping, it can be shown that the eigenvalues can be expressed as

$$\lambda_{c,i}, \lambda_{c,i}^* = -\zeta_i \omega_i \pm j \omega_i \sqrt{1 - \zeta_i^2} \tag{2.23}$$

and therefore contain all the frequency and damping ratio information. By definition the output matrix C selects the components of the mode shapes corresponding to an output location. So, each column vector in the modal output matrix $C\Psi$ defines a part of the corresponding mode shape that can be observed from the data.

To this end the state space model is expressed in continuous time, whereas in reality measurements are taken at discrete time intervals. In order to fit models to measurements (which is the aim of system identification), this model has to be converted to discrete time. For this purpose, consider first the solution to the first order differential equation of motion given by Eq. (2.15) that can be written as

$$x(t) = e^{A_c t} x(t_0) + \int_{t_0}^{t} e^{A_c (t-\tau)} B_c u(\tau) d\tau \tag{2.24}$$

where the first term on the right-hand side constitutes the initial condition response, and the second term is due to the excitation the system is exposed to. Without loss of generality, let $t_0 = 0$ and Eq. (2.24) can be rewritten as

$$x(t) = e^{A_c t} x(0) + \int_{0}^{t} e^{A_c (t-\tau)} B_c u(\tau) d\tau \tag{2.25}$$

If a sampling interval Δt is assumed, then the solution to the state equation leads to

$$x(k\Delta t) = e^{A_c k\Delta t} x(0) + \int_{0}^{k\Delta t} e^{A_c (k\Delta t-\tau)} B_c u(\tau) d\tau \tag{2.26}$$

If k is increased by 1 to $k+1$, the following expression is obtained

$$x([k+1]\Delta t) = e^{A_c k\Delta t} x(k\Delta t) + \int_{k\Delta t}^{(k+1)\Delta t} e^{A_c ([k+1]\Delta t-\tau)} B_c u(\tau) d\tau \tag{2.27}$$

Eq. (2.27) is cumbersome to use in practice due to the need to integrate for each value of k. However, if a Zero Order Hold (ZOH) assumption is imposed on the input term (i.e., $u(\tau) = u(k\Delta t)$ over the interval $k\Delta t \le \tau < (k+1)\Delta t$), the input function can be taken outside the integral, and Eq. (2.27) boils down to

$$x(k+1) = Ax(k) + Bu(k) \tag{2.28}$$

where the shorthand notation k is used instead of $k\Delta t$. Eq. (2.28) is called the discrete time state equation, and A and B are the discrete time state and input matrices that are related to their continuous time counterparts through the following relations:

$$A = e^{A_c \Delta t} = \sum_{i=0}^{\infty} \frac{A_c^i (\Delta t)^i}{i!}$$
$$B = \left(\int_0^{\Delta t} e^{A_c \tau} d\tau \right) B_c = \left(\sum_{i=0}^{\infty} \frac{A_c^i (\Delta t)^{i+1}}{i!} \right) B_c \tag{2.29}$$

The transformation to discrete time has no effect on the structure of the output matrix and the direct transmission term since they are only some mapping matrices, and thus have no contribution to the dynamics of a system. The output vector at the k^{th} time step can, therefore, be related to the discrete states (and the k^{th} input sample if the outputs contain any acceleration measurements) as

$$y(k) = Cx(k) + Du(k) \tag{2.30}$$

Eqs. (2.28) and (2.30) are together called the discrete time state space equations:

$$\begin{aligned} x(k+1) &= Ax(k) + Bu(k) \\ y(k) &= Cx(k) + Du(k) \end{aligned} \tag{2.31}$$

and as can be inferred from the discretization process, reducing Eq. (2.18) to Eq. (2.31) is in essence nothing but the conversion of a set of first order differential equations to a set of first order difference equations.

The output can be calculated from Eq. (2.31) but requires the state vector. An explicit solution that depends only on the input can, however, be obtained by means of some recursive computations. Assuming , without loss of generality, $x(0) = 0$, it can be shown that the output sequence can be expressed in terms of the matrices A, B, C, and D as

$$y(k) = \left(\sum_{i=0}^{k-1} CA^i Bu(k-1-i) \right) + Du(k) \tag{2.32}$$

Here the sequence of matrices $D, CB, CAB, CA^2B, CA^3B, \ldots$ are called the Markov parameters, and represent response of a system to a unit pulse input. Even though A, B,

C, and D need not be unique as pointed out earlier, the Markov parameters are invariant under coordinate transformations.

It is appropriate, at this point of the discussion, to establish the connections between the discrete time state space model and the modal model. Consider for this purpose the eigenvalue decomposition of the discrete state matrix A which can be found by making use of the eigenvalue decomposition of the continuous state matrix A_c and Eq. (2.29) as follows:

$$A = e^{A_c \Delta t} = e^{\Psi \Lambda_c \Psi^{-1} \Delta t} = \Psi e^{\Lambda_c \Delta t} \Psi^{-1} = \Psi \left(\sum_{i=0}^{\infty} \frac{\Lambda_c^i (\Delta t)^i}{i!} \right) \Psi^{-1} = \Psi \Lambda_d \Psi^{-1} \tag{2.33}$$

Here Λ_d is a diagonal matrix of dimensions $n \times n$, and it contains the N complex conjugate eigenvalue pairs $(\lambda_{d,i}, \lambda_{d,i}^*)$ of the discrete time state matrix A. Eq. (2.33) suggests that the discrete eigenvectors are equal to the continuous ones, and the continuous eigenvalues $\lambda_{c,i}$ are related to the discrete ones as

$$\lambda_{c,i} = \frac{\ln(\lambda_{d,i})}{\Delta t} = \frac{\ln\left(|\lambda_{d,i}| e^{j(\theta_{d,i} + 2\pi l)} \right)}{\Delta t} = \frac{\ln(|\lambda_{d,i}|)}{\Delta t} + j\left(\frac{\theta_{d,i}}{\Delta t} + \frac{2\pi l}{\Delta t} \right) \tag{2.34}$$

where $|\bullet|$ denotes absolute value operator, $\theta_{d,i}$ are the phase angles of the discrete time complex eigenvalues, and $l = 0, 1, 2, \ldots$. The second equality in Eq. (2.34) is nothing but paraphrasing the complex $\lambda_{d,i}$ in terms of the absolute value and the associated phase angle. The problem with Eq. (2.34) is that the value of l is unknown. For the rest of the discussion it will be set to zero, which is equivalent to making the assumption that all the frequencies of the continuous time signal are below the Nyquist frequency. The Nyquist frequency f_N is defined as

$$f_N = \frac{f_s}{2} = \frac{1}{2\Delta t} \tag{2.35}$$

and according to the sampling theorem constitutes the largest frequency that can be observed from a signal sampled with a sampling frequency $f_s = 1/\Delta t$. Provided that the sampling interval has been chosen small enough, the continuous time eigenvalues can be computed by means of the following relation:

$$\lambda_{c,i} = \frac{\ln\left(\left|\lambda_{d,i}\right|\right)}{\Delta t} + j\left(\frac{\theta_{d,i}}{\Delta t}\right) \tag{2.36}$$

Once the eigendecomposition of the discrete time state matrix is done, it is possible to obtain the continuous time eigenvalues and eigenvectors by Eq.(2.36). The modal frequencies and damping ratios can, then, be evaluated from these by means of Eq. (2.12).

2.2. Evolution from Deterministic to Stochastic State Space Models

The model described by Eqs. (2.18) or (2.31) is deterministic in the sense that whatever input drives the system, the response can be exactly predicted. In reality, however, there exists no such determinism, and noise is always present in the data. The noise basically stems from two sources: The uncontrolled and unmeasured inputs that the system might be subjected to during the experiment, and the sensor inaccuracies. When all these factors are integrated into the state space equations, the discrete time combined deterministic-stochastic state space model is obtained as follows:

$$\begin{aligned} x(k+1) &= Ax(k) + Bu(k) + w(k) \\ y(k) &= Cx(k) + Du(k) + v(k) \end{aligned} \tag{2.37}$$

where $w(k)$, of dimensions $n \times 1$, accounts for the process noise due to uncontrolled inputs, and $v(k)$, of dimensions $m \times 1$, represents the measurement noise. These vectors constitute the stochastic component of the model, and they are assumed to be zero mean (i.e. $\mathbf{E}\left[w(k)\right] = 0$, $\mathbf{E}\left[v(k)\right] = 0$), and white with covariance matrices expressed as

$$\mathbf{E}\left[\begin{Bmatrix} w(p) \\ v(p) \end{Bmatrix}\begin{Bmatrix} w(q)^T & v(q)^T \end{Bmatrix}\right] = \begin{bmatrix} \widehat{Q} & \widehat{S} \\ \widehat{S}^T & \widehat{R} \end{bmatrix}\delta_{pq} \tag{2.38}$$

where $\mathbf{E}[\bullet]$ denotes the expected value operator, δ_{pq} is the Kronecker delta, and p and q are two arbitrary time instants.

In the case of ambient vibrations, the input excitation remains unknown. Due to the lack of input information, it is not possible (from a system identification standpoint) to differentiate $u(k)$ from the noise terms $w(k)$ and $v(k)$. Omitting the terms containing $u(k)$ in Eq. (2.37) results in the following model:

$$\begin{aligned} x(k+1) &= Ax(k) + w(k) \\ y(k) &= Cx(k) + v(k) \end{aligned} \tag{2.39}$$

Eq. (2.39) is called the discrete time stochastic state space model in which the driving force is implicitly accounted for by the noise terms. If the whiteness assumption concerning these noise vectors is ever violated such that the input contains some dominant frequency components, these components will also be observed in the output, and hence be treated as a system mode in the identification process.

In addition to the above assumptions regarding the noise terms, the stochastic process $x(k)$ is also assumed to be zero mean and stationary:

$$\mathbf{E}[x(k)] = 0,\ \mathbf{E}\left[x(k)x(k)^T\right] = \Sigma \tag{2.40}$$

The term Σ in Eq. (2.40) is defined as the state covariance matrix, and is independent of the time step k. This is a natural result of the stationarity assumption that dictates the statistical properties of a random process to be invariant with respect to time.

Furthermore, the noise vectors $w(k)$ and $v(k)$ are assumed to be independent of the state vector $x(k)$. This assumption, coupled with the previous assumption that these vectors are zero mean, yields

$$\mathbf{E}\left[x(k)w(k)^T\right] = 0,\ \mathbf{E}\left[x(k)v(k)^T\right] = 0 \tag{2.41}$$

Defining the output covariance matrices as

$$R_i = \mathbf{E}\left[y(k+i)y(k)^T \right] \tag{2.42}$$

the state-output covariance matrix as

$$G = \mathbf{E}\left[x(k+1)y(k)^T \right] \tag{2.43}$$

and making use of the above assumptions, the following relations can be inferred:

$$\begin{aligned} \Sigma &= A\Sigma A^T + \widehat{Q} \\ R_0 &= C\Sigma C^T + \widehat{R} \\ G &= A\Sigma C^T + \widehat{S} \end{aligned} \tag{2.44}$$

$$R_i = CA^{i-1}G \tag{2.45}$$

Eq. (2.45) suggests that the output covariances can be considered analogous to the Markov parameters of a deterministic, linear, time invariant system described by A, G, C, R_0. This is an important implication in the sense that the output covariances can be used as inputs to the classical realization algorithms that are based on the factorization of Markov parameter sequences. Owing to this property, Eq. (2.45) will also have a major role in the derivation of the stochastic subspace identification algorithms that will be treated in the following section.

2.3. Stochastic Subspace Identification Algorithms

2.3.1. Problem Statement and Notation

In a structural analysis procedure, one assigns the model parameters (either the spatial characteristics such as mass, damping and rigidity or the modal parameters of the modes of interest depending on the initially assumed model), and generates the desired responses to the prescribed inputs. In system identification, on the other hand, one has the

information about the response (in some cases the input as well), and aims at deriving the assumed model's parameters based on this information.

The stochastic identification algorithms that will be considered in this study are the SSI-COV and SSI-DATA algorithms. Both algorithms work in time domain, and both try to fit stochastic state space models to the experimental data. Put more formally, the modal identification problem investigated here can be defined as the determination of the system order n, and the corresponding system matrices A and C (up to within a similarity transformation) using the available output measurements which might be composed of displacements, velocities and/or accelerations. The extraction of modal parameters from the state space matrices is then straight forward from the discussion given in Section 2.1.2.

Before proceeding with the identification algorithms, some notation needs to be introduced. The significance of the following material will be clear as the algorithms are explained.

Suppose we are given s output vectors $y(0), y(1), y(2).....y(s-1)$. These measurements can be collected in a block Hankel matrix H which has $2i$ block rows and l columns such that

$$H = \left[\begin{array}{ccccc} y(0) & y(1) & y(2) & \cdots & y(l-1) \\ y(1) & y(2) & y(3) & \cdots & y(l) \\ \vdots & \vdots & \vdots & \ddots & \vdots \\ y(i-1) & y(i) & y(i+1) & \cdots & y(i+l-2) \\ \hline y(i) & y(i+1) & y(i+2) & \cdots & y(i+l-1) \\ y(i+1) & y(i+2) & y(i+3) & \cdots & y(i+l) \\ \vdots & \vdots & \vdots & \ddots & \vdots \\ y(2i-1) & y(2i) & y(2i+1) & \cdots & y(2i+l-2) \end{array}\right] = \left[\begin{array}{c} Y_{0|i-1} \\ \hline Y_{i|2i-1} \end{array}\right] = \left[\begin{array}{c} Y_p \\ \hline Y_f \end{array}\right] \quad (2.46)$$

The subscripts of $Y_{i|2i-1}$ stand for the time indices corresponding to the first and last elements in the first column of the block data Hankel matrix. The matrices Y_p and Y_f, both of dimensions $im \times l$, are obtained by splitting H into two matrices with i block rows each, and the subscripts denote "past" and "future", respectively. The integer i should be

chosen such that $im \geq n$, and for obvious reasons l could at most be equal to $s - 2i + 1 \geq n$ (for statistical reasons that will be clear later on, it is assumed that $l \to \infty$).

The derivation of the SSI-DATA algorithm requires two other data matrices to be defined by shifting the border between past and future one block row down which reads

$$Y_p^+ = Y_{0|i},\ Y_f^- = Y_{i+1|2i-1} \tag{2.47}$$

where Y_p^+ and Y_f^- have dimensions $(i+1)m \times l$ and $(i-1)m \times l$ in this case.

The identification algorithms of the following sections make extensive use of the observability and controllability matrices. The observability matrix O_i is defined as

$$O_i = \begin{bmatrix} C \\ CA \\ CA^2 \\ \vdots \\ CA^{i-1} \end{bmatrix} \tag{2.48}$$

and has dimensions $im \times n$. If a system is observable, it means that all the modes of the system can be observed in the output and $rank(O_i) = n$. The reversed stochastic controllability matrix Γ_i, on the other hand, is defined as

$$\Gamma_i = \begin{bmatrix} A^{i-1}G & A^{i-2}G & A^{i-3}G & \cdots & AG & G \end{bmatrix} \tag{2.49}$$

and is an $n \times im$ matrix. If a system is controllable, this implies that all the modes of the system can be excited by the stochastic input and $rank(\Gamma_i) = n$ (Kailath, 1980).

2.3.2. Covariance-Driven Stochastic Subspace Identification

This section introduces the covariance-driven stochastic subspace identification. This is also addressed as the stochastic realization problem which was first solved by Akaike (1974).

The algorithm starts with the formation of a Toeplitz matrix T_i composed of output covariances:

$$T_i = \begin{bmatrix} R_i & R_{i-1} & \cdots & R_2 & R_1 \\ R_{i+1} & R_i & \cdots & R_3 & R_2 \\ \vdots & \vdots & \ddots & \vdots & \vdots \\ R_{2i-1} & R_{2i-2} & \cdots & R_{i+1} & R_i \end{bmatrix} \tag{2.50}$$

Assuming ergodicity, which dictates that the expected value of a stationary process can be replaced by the average over one infinitely long record of the process, Eq. (2.42) can be rewritten as follows:

$$R_i = \mathbf{E}\left[y(k+i)y(k)^T \right] = \lim_{l\to\infty} \frac{1}{l} \sum_{k=0}^{l-1} y(k+i)y(k)^T \tag{2.51}$$

In reality, only a finite number of samples are available and only estimates of the output covariances can be obtained by dropping the limit on the second expression in Eq. (2.51) as

$$R_i \approx \frac{1}{l} \sum_{k=0}^{l-1} y(k+i)y(k)^T \tag{2.52}$$

Therefore, a fast way of computing an estimate for T_i is obvious from the definitions given in Eqs. (2.46) and (2.52):

$$T_i = \frac{1}{l} Y_f Y_p^T \tag{2.53}$$

Making use of the property introduced in Eq. (2.45) along with the definitions given in Eqs. (2.48) and (2.49), T_i can be decomposed as

$$T_i = \begin{bmatrix} C \\ CA \\ \vdots \\ CA^{i-1} \end{bmatrix} \begin{bmatrix} A^{i-1}G & A^{i-2}G & \cdots & AG & G \end{bmatrix} = O_i \Gamma_i \tag{2.54}$$

If $im \geq n$, and the system is both observable and controllable, the rank of the Toeplitz matrix, which has dimensions $im \times im$, should be equal to n. This follows from Eq. (2.54) where T_i is found to be the product of two matrices each having rank n.

Eq. (2.54) brings along the question of determining the rank of the covariance matrix T_i. Singular Value Decomposition (SVD) is a numerically robust tool that could be used for this purpose. Applying SVD to T_i yields

$$T_i = USV^T = \begin{bmatrix} U_1 & U_2 \end{bmatrix} \begin{bmatrix} S_1 & 0 \\ 0 & 0 \end{bmatrix} \begin{bmatrix} V_1^T \\ V_2^T \end{bmatrix} = U_1 S_1 V_1^T \tag{2.55}$$

where $U_{im \times im}$ and $V_{im \times im}$ are orthonormal matrices, and $S_{im \times im}$ is a diagonal matrix with the positive singular values (in descending order) as its entries. The practical interpretation of this rank determination process corresponds to finding out the number of independent vibration modes that satisfactorily characterize a linear dynamic system while truncating those that have insignificant contribution to the overall response or that are not actual structural modes at all.

A special note should be added at this point of the discussion concerning this rank determination operation via SVD. In reality, none of the singular values in Eq. (2.55) will be exactly zero due to the measurement noise inherent in the data. Therefore, a need arises to distinguish these noise modes from the actual system modes. This problem is usually referred to as spurious or mathematical mode discrimination in the literature. A simple way to tackle the problem is to try to find a gap between the singular values. However, there

might be occasions where it is hard to find such a clear gap, and one needs more reliable tools in these cases. This discussion will be detailed in the following sections where the identification algorithms are applied to a variety of systems involving different levels of complexity; and some pole selection strategies will be suggested in the context of this applied study.

Combining the expressions in Eqs. (2.54) and (2.55), it is possible to achieve a realization of the observability and the reversed stochastic controllability matrices as

$$\begin{aligned} O_i &= U_1 S_1^{1/2} \\ \Gamma_i &= S_1^{1/2} V_1^T \end{aligned} \tag{2.56}$$

Eq. (2.56) is referred to as the Balanced Realization (BR). The BR algorithm makes use of the principal components of the covariance matrix T_i (Arun and Kung, 1990). The particular state space realization resulting from the procedure is balanced in the sense that O_i and Γ_i both have orthogonal columns and

$$O_i^T O_i = \Gamma_i \Gamma_i^T = S_1 \tag{2.57}$$

From the definitions of the observability and controllability matrices, it is straight forward that the output matrix C is the first m rows of O_i, and the state-output covariance matrix G is the last m columns of Γ_i. The state matrix A can be found by making use of the shift structure of the observability matrix as

$$A = \underline{O}_i^{\dagger} \overline{O}_i \tag{2.58}$$

where $\underline{O}_i$ and $\overline{O}_i$ denote the observability matrix with the last and first m rows truncated, respectively, and $(\bullet)^{\dagger}$ is the Moore-Penrose matrix pseudo-inverse. The zero-lag output covariance matrix R_0 can, then, be computed as

$$R_0 = \frac{1}{l}\sum_{k=i}^{i+l-1} y(k)y(k)^T = \frac{1}{l}Y_{i|i}Y_{i|i}^T \tag{2.59}$$

It is important to note that the state output covariance matrix G, and the zero-lag output covariance matrix R_0 have no significance in terms of modal parameter estimation. Their identification has been shown here only for the sake of completeness of the derivation.

Along similar lines of reasoning, there exists other realization algorithms published in the literature. One such algorithm is the Canonical Variate Analysis (CVA) (Akaike, 1975) the implementation of which can be easily fitted within the framework of the above explained algorithm by introducing some weighting matrices to Eq. (2.50) such that

$$\left(T_i\right)_W = W_1 T_i W_2 \tag{2.60}$$

In CVA, it is aimed at normalizing the data such that the singular values of the weighted Toeplitz matrix $\left(T_i\right)_W$, of dimensions $im \times im$, lie between 0 and 1. In this fashion, the singular values represent the cosines of the angles between the subspaces of Y_p and Y_f. This approach is particularly useful when the system order is not known because it minimizes the effects of noise modes while amplifying those of the system modes, thereby reducing numerical problems (Guyader and Mevel, 2003). The weighting matrices W_1 and W_2 can be chosen as

$$W_1 = \left(\frac{1}{l}Y_f Y_f^T\right)^{-1/2},\ W_2 = \left(\frac{1}{l}Y_p Y_p^T\right)^{-1/2} \tag{2.61}$$

so that the norm of the weighted Toeplitz matrix $\left(T_i\right)_W$ is equal to 1.

The only difference of CVA with respect to BR is in the realization step given by Eq. (2.56). The observability and controllability matrices are realized in this algorithm as follows:

$$O_i = W_1^{-1} U_1 S_1^{1/2}$$
$$C_i = S_1^{1/2} V_1^T W_2^{-1} \tag{2.62}$$

The rest of the procedure (i.e., the computation of the state space matrices) is identical to the one explained for the BR algorithm. The flow chart presented in summarizes all the computational steps of the SSI-COV algorithm.

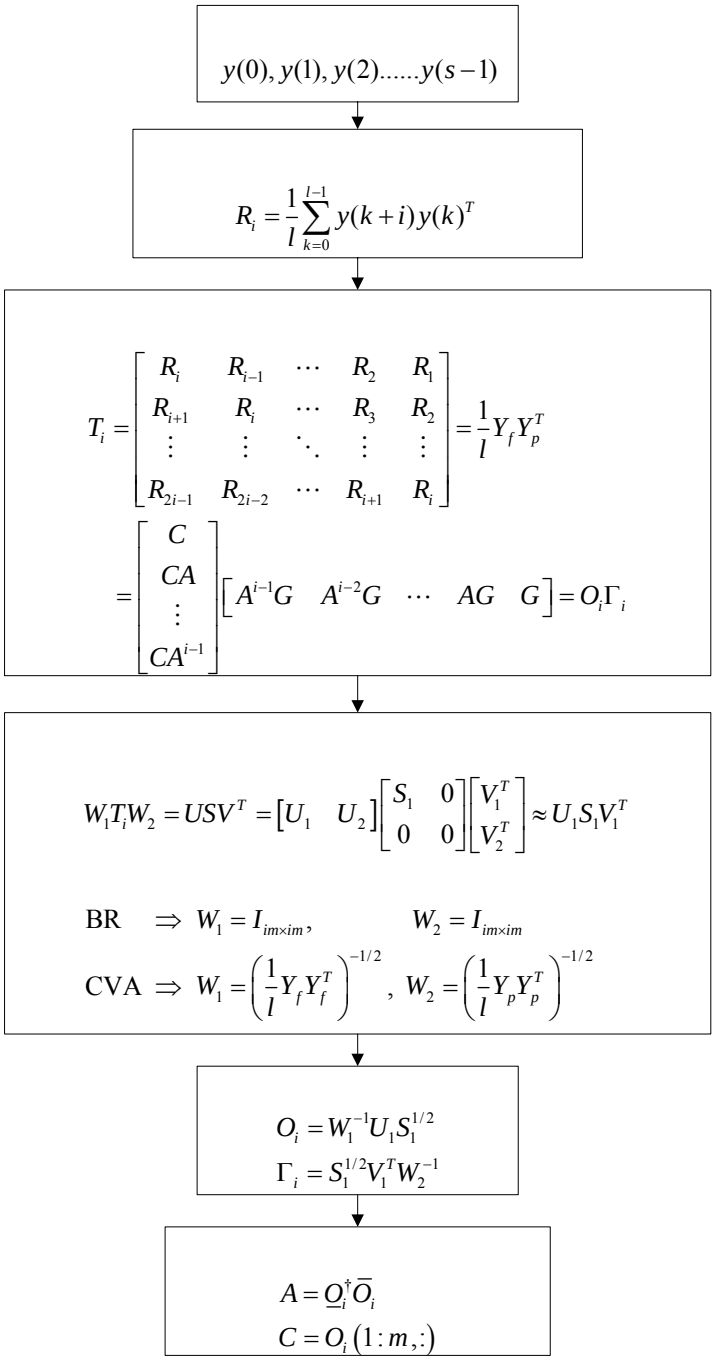

Figure 2.1. Flowchart for the SSI-COV algorithm

2.3.3. Data-Driven Stochastic Subspace Identification

The main difference of the SSI-DATA from the previous algorithm is that it operates directly on the output data sequence, and computes the output covariances implicitly through matrix projections (Viberg, 1995). The second important novelty regarding this algorithm is that it identifies a set of Kalman filter state estimates, and the state-space matrices are computed in a least squares sense using these states and the output data.

The algorithm starts with the orthogonal projection of the row space of Y_f into the row space of Y_p. This projection is defined as

$$P_i = Y_f / Y_p = Y_f Y_p^T \left(Y_p Y_p^T \right)^{\dagger} Y_p \tag{2.63}$$

and, in practice, can be interpreted as an 'improved estimate' of Y_f whereby the noise component orthogonal to Y_p is removed. The projection operation can, indeed, be viewed as the counterpart of the explicit covariance estimation step involved in the SSI-COV algorithm. The actual implementation can easily be performed by means of the QR-decomposition. If the block data Hankel matrix in Eq. (2.46) is factorized such that

$$\begin{bmatrix} Y_{0|i-1} \\ Y_{i|i} \\ Y_{i+1|2i-1} \end{bmatrix} = \begin{bmatrix} R_{11} & 0 & 0 \\ R_{21} & R_{22} & 0 \\ R_{31} & R_{32} & R_{33} \end{bmatrix} \begin{bmatrix} Q_1^T \\ Q_2^T \\ Q_3^T \end{bmatrix} \tag{2.64}$$

where $Q_{l\times 2im}$ is an orthonormal matrix, and $R_{2im\times 2im}$ is a lower triangular matrix; the projection defined in Eq. (2.63) can be extracted from this factorization as follows:

$$P_i = \begin{bmatrix} R_{21} \\ R_{31} \end{bmatrix} Q_1^T \tag{2.65}$$

It can be shown that the matrix P_i, of dimensions $im \times l$, is equal to the product of the observability matrix O_i, and a matrix $\hat{X}_i$ that contains certain Kalman filter states and has dimensions $n \times l$:

$$P_i = O_i \hat{X}_i = \begin{bmatrix} C \\ CA \\ \vdots \\ CA^{i-1} \end{bmatrix} \begin{bmatrix} \hat{x}_i & \hat{x}_{i+1} & \cdots & \hat{x}_{i+l-1} \end{bmatrix} \tag{2.66}$$

The proof for Eq. (2.66) has been provided by Van Overschee and De Moor (1996). Since the projection matrix P_i is found to be the product of two matrices with rank n, its rank should also equal n. The SVD of P_i yields

$$P_i = USV^T = \begin{bmatrix} U_1 & U_2 \end{bmatrix} \begin{bmatrix} S_1 & 0 \\ 0 & 0 \end{bmatrix} \begin{bmatrix} V_1^T \\ V_2^T \end{bmatrix} = U_1 S_1 V_1^T \tag{2.67}$$

and the rank can be decided upon the number of nonzero singular values in Eq. (2.67).

The observability matrix O_i and the Kalman filter state sequence $\hat{X}_i$ can then be recovered as

$$\begin{aligned} O_i &= U_1 S_1^{1/2} \\ \hat{X}_i &= O_i^{\dagger} P_i \end{aligned} \tag{2.68}$$

In order to extract the system matrices, one more Kalman filter state sequence $\hat{X}_{i+1}$ should be realized, and this can be achieved by computing another projection similar to the one given in Eq. (2.66) which yields

$$P_{i-1} = Y_f^- / Y_p^+ = O_{i-1}\hat{X}_{i+1} = \begin{bmatrix} C \\ CA \\ \vdots \\ CA^{i-2} \end{bmatrix} \begin{bmatrix} \hat{x}_{i+1} & \hat{x}_{i+2} & \cdots & \hat{x}_{i+l} \end{bmatrix} \tag{2.69}$$

The projection matrix P_{i-1} has dimensions $m(i-1)\times l$ this time, and can be retrieved from Eq. (2.64) as

$$P_{i-1} = \begin{bmatrix} R_{31} & R_{32} \end{bmatrix} \begin{bmatrix} Q_1^T \\ Q_2^T \end{bmatrix} \tag{2.70}$$

The state sequence $\hat{X}_{i+1}$ can then be evaluated by the following equality

$$\hat{X}_{i+1} = O_{i-1}^{\dagger} P_{i-1} \tag{2.71}$$

where O_{i-1} is the observability matrix with the last m rows truncated.

Now that the system order and the state sequences are determined, the system matrices can be computed by solving the following set of equations in a least squares sense:

$$\begin{bmatrix} \hat{X}_{i+1} \\ Y_{i|i} \end{bmatrix} = \begin{bmatrix} A \\ C \end{bmatrix} \hat{X}_i + \begin{bmatrix} \varepsilon_w \\ \varepsilon_v \end{bmatrix} \tag{2.72}$$

The matrices ε_w and ε_v are simply the least squares residuals, and has respective dimensions $n\times l$ and $m\times l$. These residual matrices can be used to compute the error covariance matrices defined in Eq. (2.38) as

$$\begin{bmatrix} \widehat{Q} & \widehat{S} \\ \widehat{S}^T & \widehat{R} \end{bmatrix} = \begin{bmatrix} \varepsilon_w \\ \varepsilon_v \end{bmatrix} \begin{bmatrix} \varepsilon_w^T & \varepsilon_v^T \end{bmatrix} \tag{2.73}$$

Finally, the state-output covariance matrix G, and the zero-lag output covariance matrix R_0 can be computed using the relations in Eq. (2.44). It should be mentioned that the covariance sequence determined by thus identified A, C, G, R_0 is a positive real sequence.

With the inclusion of minor modifications, the BR and CVA algorithms can be implemented into the SSI-DATA scheme. The modification involves introducing some weighting matrices into Eq. (2.63) such that the weighted projection matrix has the form

$$\left(P_i\right)_W = W_1 P_i W_2 \tag{2.74}$$

The observability matrix O_i and the Kalman filter states $\hat{X}_i$ can then be computed by means of the SVD of $\left(P_i\right)_W$ as

$$\begin{aligned} O_i &= W_1^{-1} U_1 S_1^{1/2} \\ \hat{X}_i &= O_i^{\dagger} P_i \end{aligned} \tag{2.75}$$

The appropriate weighting matrices can be selected as

$$W_1 = I,\ W_2 = Y_p^T \left(Y_p Y_p^T\right)^{-1/2} Y_p \tag{2.76}$$

for the BR algorithm and

$$W_1 = \left(Y_f Y_f^T\right)^{-1/2},\ W_2 = I_{l \times l} \tag{2.77}$$

for the CVA, respectively. A schematic overview of the SSI-DATA algorithm has been provided in Figure 2.2.

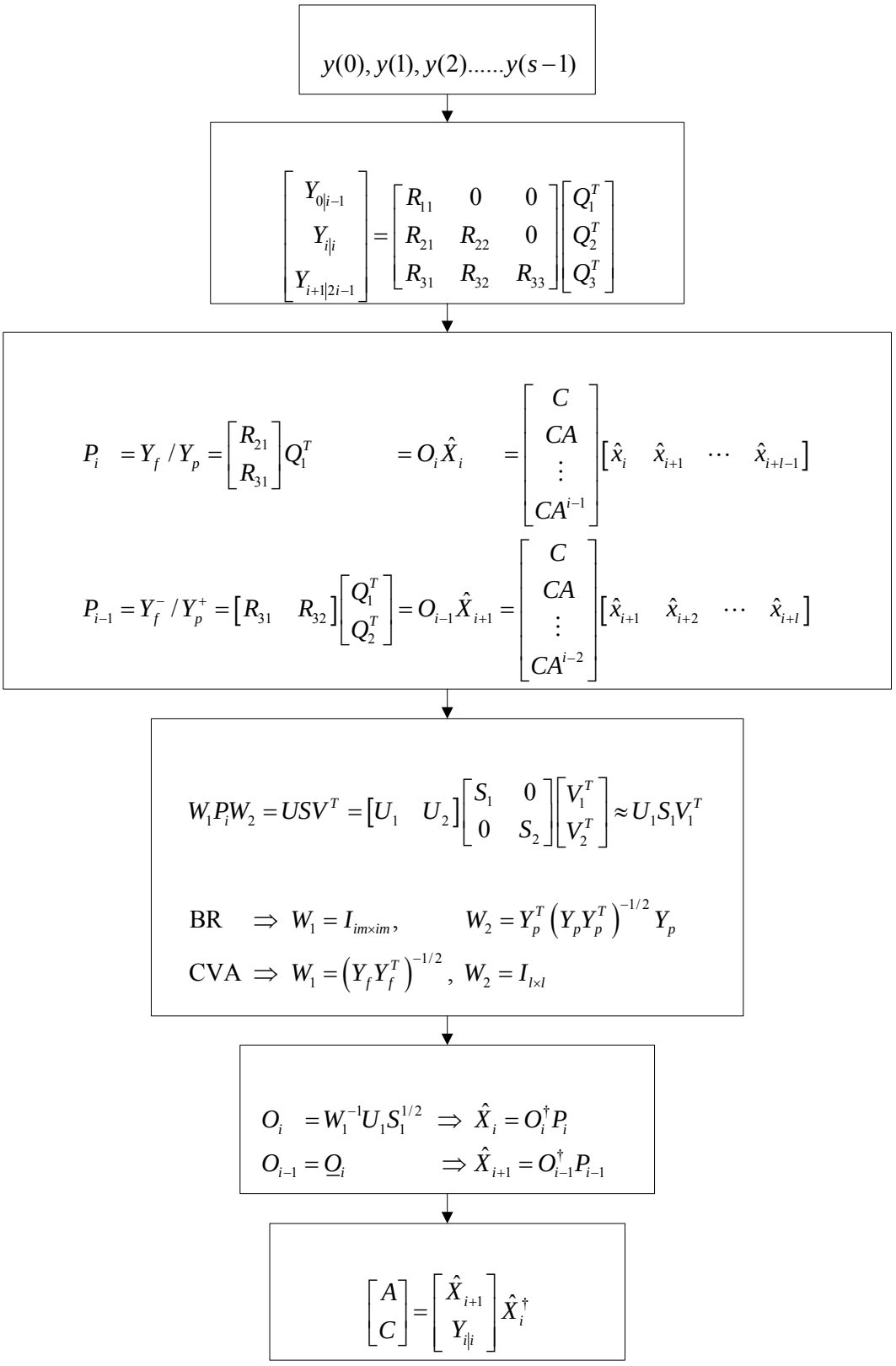

Figure 2.2. Flowchart for the SSI-DATA algorithm

3. CASE STUDIES

3.1. Numerical Example

The first step in the analysis is to compare the modal parameter identification capabilities of the subspace algorithms via the 3-DOF spring-dashpot model illustrated in Figure 3.1. The corresponding mass and stiffness matrices are given in Table 3.1, and the modal damping ratios are assigned as $\zeta_1 = 2\%$, $\zeta_2 = 8\%$ and $\zeta_3 = 4\%$.

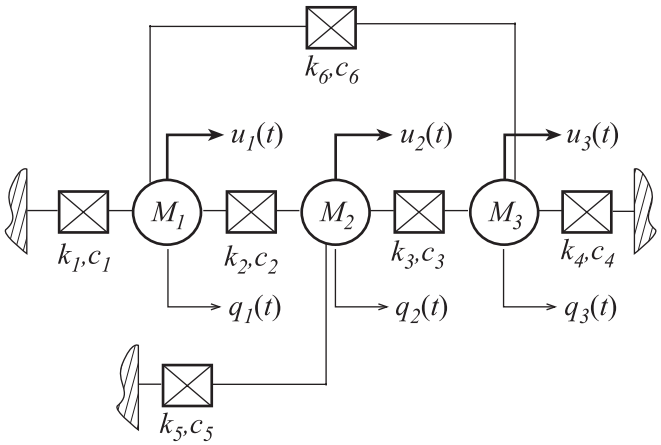

Figure 3.1. Spring-dashpot model

Table 3.1. Mass and stiffness matrices for the 3-DOF spring-dashpot model

Mass			Stiffness		
0.8	0.0	0.0	40.0	-10.0	-10.0
0.0	1.2	0.0	-10.0	40.0	-10.0
0.0	0.0	2.0	-10.0	-10.0	40.0

A Monte Carlo experiment, similar to the one described by Peeters (2000), has been designed for carrying out the comparison. An individual simulation in such an experiment involves the realization of three independent Gaussian white noise sequences used to excite the model (one at each DOF). Acceleration responses from all the DOFs are then used to feed the SSI-COV (BR), SSI-COV (CVA), SSI-DATA (BR), and SSI-DATA (CVA) algorithms. The initial model order is chosen to be $n = 180$ and, though not realistic, the order is then always reduced to the true system order $n = 6$. Finally, modal parameters are estimated using the identified state space matrices. If the number of these simulations is

sufficiently large, a Monte Carlo experiment can be expected to provide useful information on the statistical properties of these estimates such as the bias and variance.

Figure 3.2 and Figure 3.3 illustrate the observed frequency histograms of the identified natural frequencies and modal damping ratios from 150 different simulations. The ordinate of these plots represent the number of observations corresponding to the interval defined in the abscissa. The estimates are normalized with respect to the actual values, so a mean value close to one represents an estimate with low bias. Similarly, the range for the x-axis is adjusted to be the same in both plots (except for two results corresponding to the second mode which involve large bias and variance) in order to enable a comparison between the relative variances of the estimates resulting from different algorithms. The continuous line superimposed to the histograms represents a normal distribution fit to the simulation results. This facilitates a better visualization of the associated bias and variance properties.

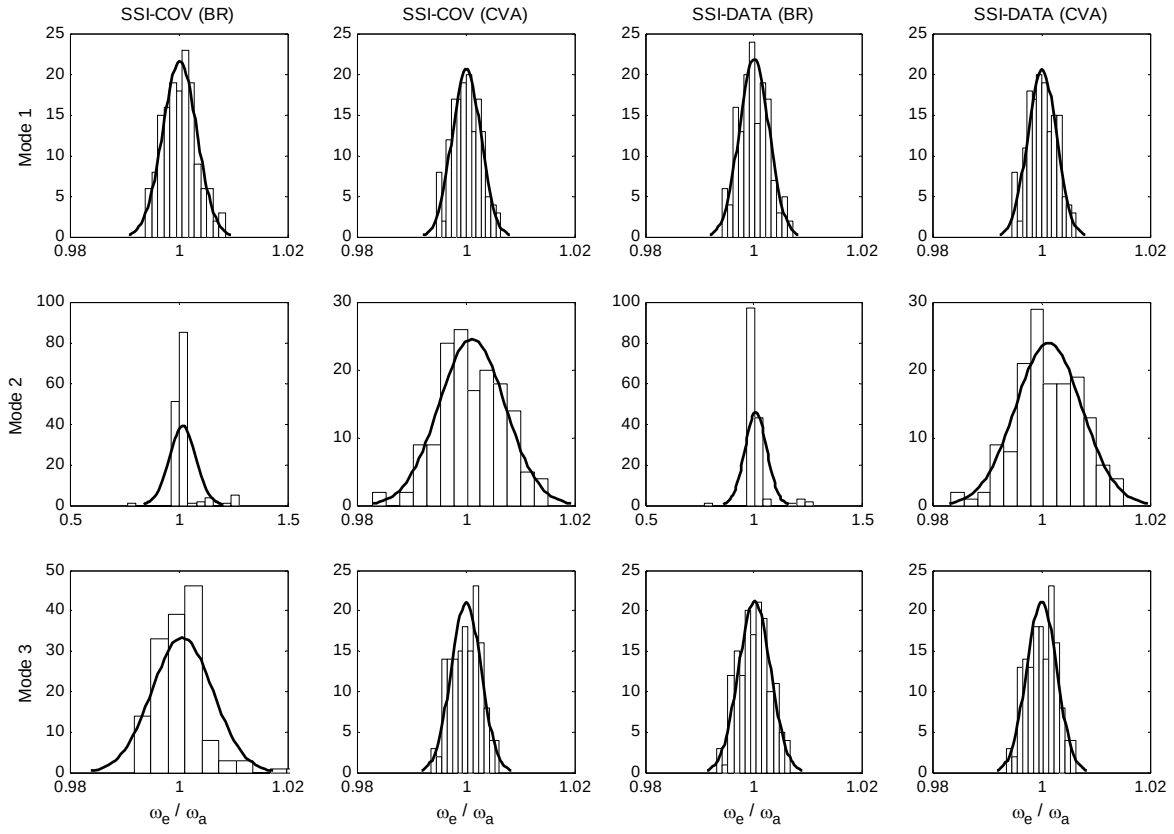

Figure 3.2. Observed frequency histograms for the natural frequency estimation results from 150 simulations. ω_e and ω_a denote the estimated and the actual natural frequencies.

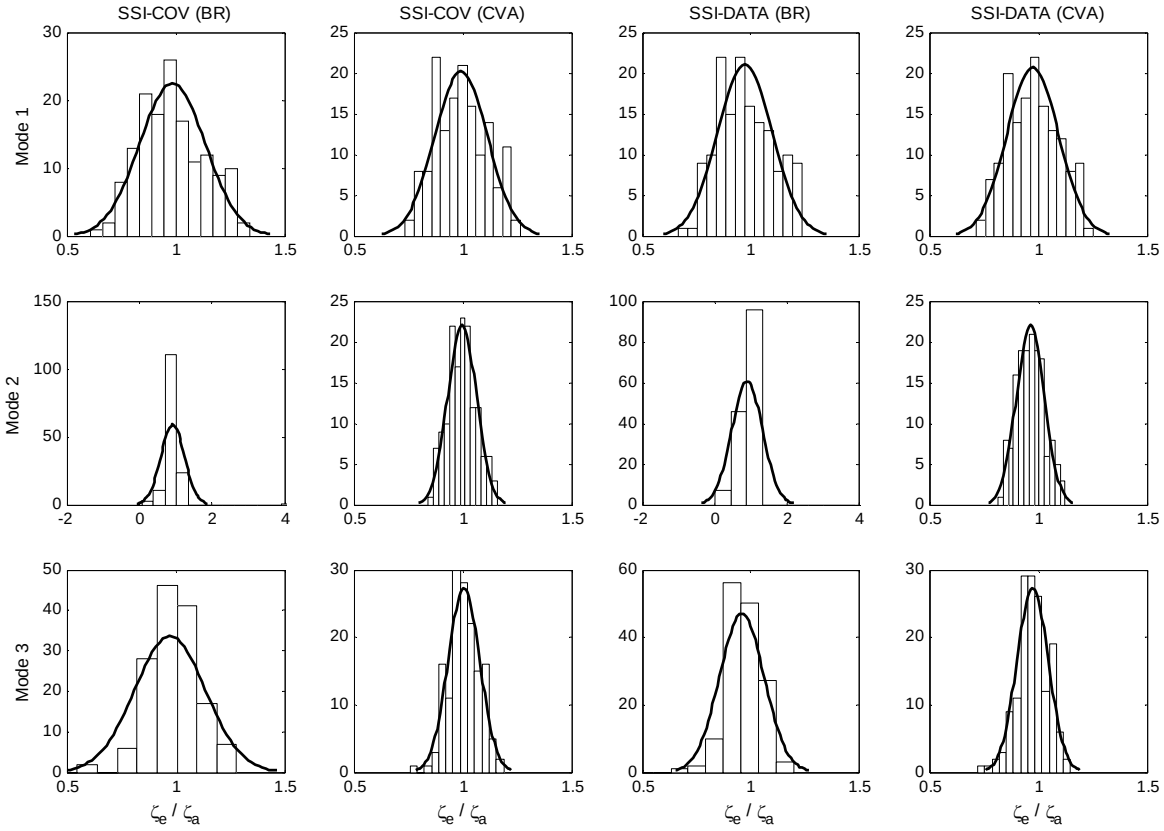

Figure 3.3. Observed frequency histograms for the damping ratio estimation results from 150 simulations. ζ_e and ζ_a denote the estimated and the actual modal damping ratios.

A summary of the results is also presented in Table 3.2, wherein the mean and the coefficient of variation (δ) values for the estimated frequencies, damping ratios and Modal Amplitude Coherence (MAC) values are reported. MAC is computed using the estimated mode shapes and the actual ones as

$$MAC\left(\psi_e,\psi_a\right)=\frac{\left|\psi_e^H\psi_a\right|^2}{\left(\psi_e^H\psi_e\right)\left(\psi_a^H\psi_a\right)} \tag{3.1}$$

where ψ_e and ψ_a are the estimated and the actual (complex) modal vectors, and $\left(\bullet\right)^H$ denotes complex transpose. Therefore, MAC is a scalar between 0 and 1, and shows the degree to which two vectors are correlated.

Table 3.2. Modal parameter estimation results from 150 simulations

Method	ω (rad/sec)		ζ (%)		MAC	
	Mean	δ (%)	Mean	δ (%)	Mean	δ (%)
Actual	3.71	-	2	-	-	-
	5.84	-	8	-	-	-
	7.45	-	4	-	-	-
SSI-COV (BR)	3.71	0.3	1.97	15.2	1.00	0.0
	5.97	5.9	7.36	35.6	0.93	22.5
	7.45	0.6	3.86	21.4	1.00	3.5
SSI-COV (CVA)	3.71	0.3	1.98	12.2	1.00	0.0
	5.85	0.6	7.98	6.6	1.00	0.2
	7.45	0.3	4.02	7.3	1.00	0.0
SSI-DATA (BR)	3.71	0.3	1.95	12.9	1.00	0.0
	5.91	5.0	7.30	46.7	0.97	12.6
	7.45	0.3	3.83	12.5	1.00	3.8
SSI-DATA (CVA)	3.71	0.3	1.95	12.2	1.00	0.0
	5.85	0.6	7.72	6.7	1.00	0.3
	7.45	0.3	3.90	7.4	1.00	0.0

The results indicate that both covariance and data driven algorithms yield similar results as far as modal parameter estimation accuracy is concerned. In fact, this is not an unexpected result in that both algorithms are based on factorization of output covariances computed either explicitly through matrix multiplications or implicitly by means of data projections. Another important observation is that the application of the CVA weighting improves the modal parameter estimates of both algorithms. It should also be noted that regardless of the algorithm and weighting used, there is, in general, a higher bias associated with the damping estimates when compared with the frequencies and the mode shape correlations. Similar results were also reported by Peeters (2000).

3.2. Phase II IASC-ASCE SHM Benchmark Problem

In order to assess the relative performances of existing SHM techniques, a task group of the American Society of Civil Engineers (ASCE) and the International Association of Structural Control (IASC) has defined a series of benchmark problems. The problem consists of an analytical and an experimental phase both of which are described in the following sections.

The structure selected for this purpose is the 4-story, 2-bay by 2-bay steel frame shown in Figure 3.4. It is located in the Earthquake Research Laboratory at the University of British Columbia. The structure is 2.5 by 2.5 in plan, and has a story height of 0.9 m, which sums up to 3.6 m for the entire structure. There are nine vertical columns that are B100×9 sections, and the floor beams are of type S75×11 sections. Each bay also consists of a diagonal bracing made of 12.7 mm diameter threaded steel rods. As for the support conditions, the vertical columns are bolted to a steel base frame and the lower flanges of these base beams are embedded in a concrete slab. So the structure may be assumed as fixed supported at the base. To make the mass distribution reasonably realistic, one heavy slab is placed in each bay per floor. Additionally, on each floor two of the masses were placed eccentrically with respect to the center. In this manner, the mass and stiffness centers are not allowed to overlap; hence some coupling between translational motions is expected.

Figure 3.4. The steel frame used for the ASCE SHM benchmark problem (ASCE SHM benchmark website, 2006)

In the analytical phase of the benchmark problem, the intent is to create a mathematical idealization of the actual structure. There exists, however, slight differences between the analytical and the actual models which will also be revealed in the identification results. These variations might be attributed to the structural properties of the diagonals, and the floor masses that have different values in each phase.

3.2.1. Analytical Phase

Within the context of the analytical phase of the benchmark problem (Bernal et al., 2002), a FE model of the benchmark structure has been developed by the SHM task group. (The FE and simulation codes can be obtained from the ASCE benchmark website). The model originally has 216 DOFs (3 translations and 3 rotations per each node excluding those at the base which are restrained from any movement) but, assuming that floors are rigid in translation along the horizontal plane and rotation about the vertical direction, the total number of DOFs has been reduced to 120.

The simulated data is generated by exciting the 120 DOF model with broadband ambient inputs applied at the geometric center of each floor along the East-West (E-W) and North-South (N-S) directions shown in Figure 3.5. At each story level, two acceleration measurements are collected in the E-W and two in the N-S direction, making a total of 16 output measurements. The data is sampled with 250 Hz for 200 seconds which in turn yields 50000 samples per output channel. White noise sequences with root mean square (RMS) values equal to 10% of the RMS of the strongest signal are then superimposed to the data as measurement noise.

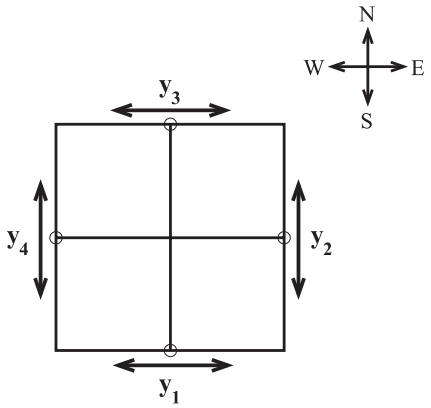

Figure 3.5. Measurement setup for the Phase II analytical benchmark problem

The system order is known in advance for this analytical model, but an effort will be made for order determination as if it were not known. Although theoretically sound, order determination via SVD has not proven to be very effective when working with ambient data, and the system order has to be inferred based on some auxiliary criteria. Arguably,

the most popular approach for differentiating system modes from spurious noise modes is working with "stabilization diagrams" (Basseville et al., 2001). A stabilization diagram is simply a plot of various model orders versus the natural frequencies identified at each of these orders (See, for instance, Figure 3.6). The motivation is that a system mode should show up with consistent frequency, damping and mode shape at various model orders, whereas the spurious ones could be expected to show a somewhat erratic behavior.

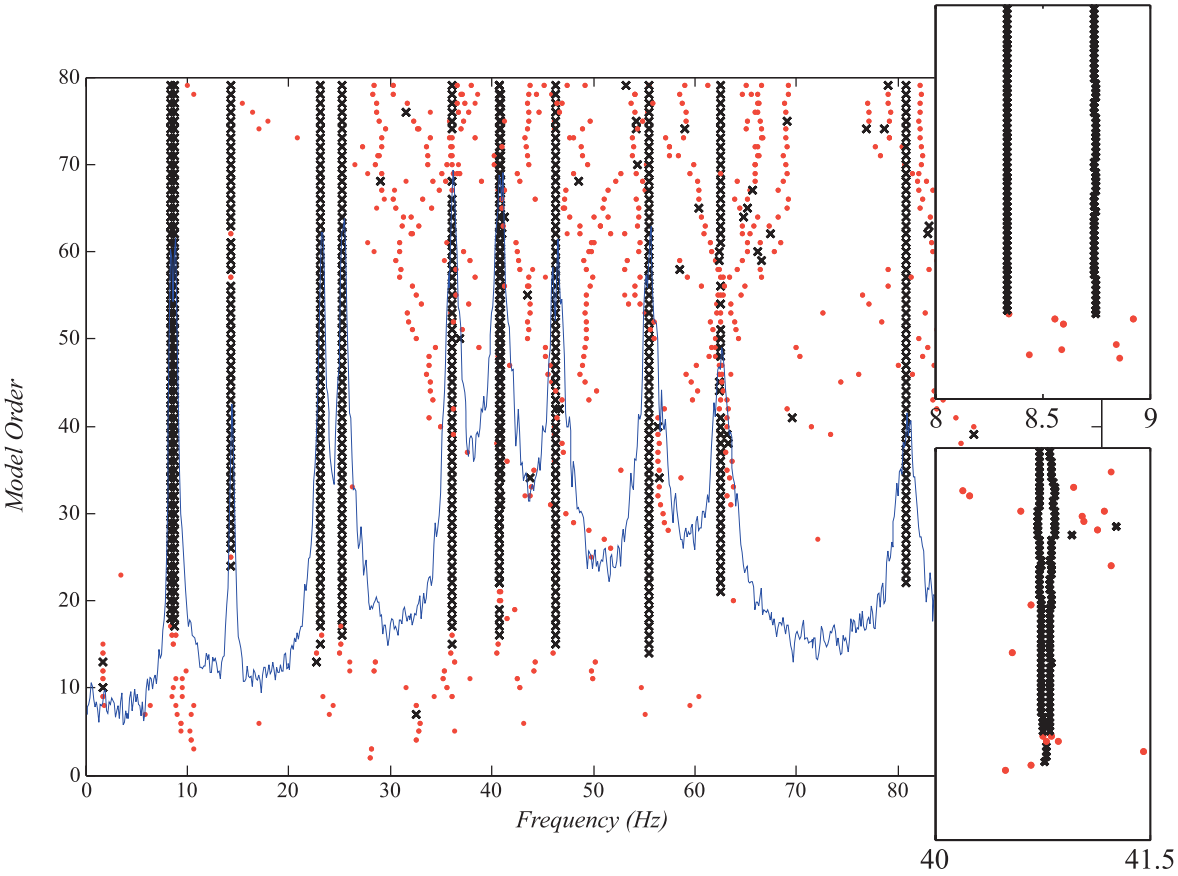

Figure 3.6. Stabilization diagram for the Phase II analytical benchmark problem. "×" and "●" denote stable and unstable modes, respectively.

The actual implementation of this strategy can be executed by initially choosing a sufficiently high order $n = im$ to be used in Eq. (2.50) or Eq. (2.66), and then constructing smaller order models by gradually reducing the number of singular values retained. This procedure yields a set of modal parameters for each consecutive order. Then, parameters that belong to two consecutive model orders are compared according to some preset criteria such as

$$\frac{\omega_p - \omega_{p+1}}{\omega_p} < \rho_\omega, \ \frac{\zeta_p - \zeta_{p+1}}{\zeta_p} < \rho_\zeta, \ 1 - MAC\left(\psi_p, \psi_{p+1}\right) < \rho_{MAC} \tag{3.2}$$

where p is the number of retained singular values (and hence the model order); ω_p, ζ_p and ψ_p are the frequency, damping ratio and (complex) mode vector estimates at this order; and ρ_ω, ρ_ζ and ρ_{MAC} are some user specified tolerance limits for labeling a modal parameter as stable. Eq. (3.2) is repeated for all available sets of modal parameters identified at each order in a sequential manner, and finally, the resulting "stable" frequencies are plotted against their corresponding model orders.

Even though stabilization diagrams prove to be useful in practical cases, the large amount of user interaction requirement is the main drawback about this procedure (Van der Auwaraer, 2001). The sequential procedure involved in its construction can also interrupt proper grouping of the stable modes. In order to overcome these difficulties, and to somewhat automate the selection process; a clustering algorithm can be adopted to select the most reliable modes from the large set of parameters identified at various model orders (Goethals et al., 2004).

In this approach, one single set of modal estimates (a frequency and the associated damping ratio and mode shape) is chosen among all the available parameters identified, and all sets which are closer to this point than a certain "radius" are clustered based on a distance measure between frequencies and damping estimates as well as the corresponding MAC values such that

$$\sqrt{\frac{1}{\Delta_\omega}(\omega_\alpha - \omega_\beta)^2 + \frac{1}{\Delta_\zeta}(\zeta_\alpha - \zeta_\beta)^2} \le \tau, \ \ 1 - MAC\left(\psi_\alpha, \psi_\beta\right) < \Delta_{MAC} \tag{3.3}$$

Here Δ_ω, Δ_ζ and Δ_{MAC} are user specified parameters analogous to the tolerance limits in Eq. (3.2), and τ is the threshold value for the "distance" between frequencies and dampings. The indices α and β in Eq. (3.3) do not denote the model order as in Eq. (3.2) but are just dummy indices that stand for two different sets of estimates. (In any case, however, attention should be paid not to include two sets of parameters that have been

identified at the same model order in the same cluster). Once such a cluster is formed, the algorithm proceeds in the same manner with the set of parameters that are left out from the previous analysis. Finally, those clusters that have a predefined number of members (e.g. a certain fraction of the total number of reduced model orders) are classified as system modes.

As can be inferred from the description of the algorithms, the main difference of the two mode selection strategies is that the stabilization procedure proceeds in a sequential manner while the clustering analysis makes use of the available data all at once, thereby rendering it more suitable for automation of the process. The clustering analysis could be used on its own, i.e. ignoring the stabilization procedure described by Eq. (3.2), or as a tool to further refine the results obtained in the stabilization procedure by only considering those modes that are labeled as "stable", thus decreasing the computation time.

Due to its relatively better performance in the Monte Carlo experiment, the SSI-DATA (CVA) algorithm is used in the analysis of the simulated data from the Phase II benchmark problem. The integer i in Eq. (2.46) is chosen as 18 so that a maximum of $n = 288$ states can be identified. This model is then reduced to $n = 2,3,...,288$, respectively. A first refinement on the identified set of modal parameters is achieved by considering their stabilization behavior with $\rho_\omega = 1\%$, $\rho_\zeta = 4\%$ and $\rho_{MAC} = 1\%$. The idea of allowing larger uncertainty for damping estimates is based on the results obtained in the previously discussed Monte Carlo experiment. The associated stabilization diagram is given in Figure 3.6. A visual inspection of this diagram reveals 12 modes (including 2 pairs of closely spaced modes presented in more detail in the subfigures) that show consistency at all selected model orders. The continuous line superimposed to the diagram represents the power spectral density (PSD) of the output estimated using Welch's modified periodogram method (Stoica and Moses, 2005). It is presented here for comparison purposes since the peaks of the PSD also correspond to the resonance frequencies of the structure.

The modal parameters that have been labeled as stable in this analysis are then subjected to the clustering analysis, the results of which are presented in Table 3.3. Here

the related tolerance parameters are imposed as $\Delta_{\omega} = 0.5\%$, $\Delta_{\zeta} = 0.05\%$, $\Delta_{MAC} = 0.01$ and the corresponding threshold value for the distance is $\tau = 1$. The proper choice of these tolerance values is, in fact, the most crucial step in this analysis because too stringent limits will cause either splitting of a system mode or misclassification of it as spurious, whereas loose limits will introduce false modes as system modes. Initially setting relatively tight limits and then combining the modes that are suspected to have split in the analysis may be a remedy to avoid these misinterpretations. In any case, the selection of the proper threshold values requires some trial and error approach. Table 3.3 shows that the frequencies form dense clusters, as can be deduced from the low coefficient of variation values associated with them, and that the damping estimates show larger deviations with respect to the mean values, similar to the Monte Carlo experiment results.

Table 3.3. Clustering analysis results for the Phase II analytical benchmark problem

Mode #	Type	ω (Hz)			ζ (%)		
		Actual	Mean	δ (%)	Actual	Mean	δ (%)
1	Bending (E-W)	8.35	8.34	0.03	1.00	0.88	4.3
2	Bending (N-S)	8.74	8.75	0.05	1.00	0.93	4.6
3	Torsion	14.34	14.33	0.08	1.00	0.82	10.0
4	Bending (E-W)	23.15	23.15	0.02	1.00	0.92	2.9
5	Bending (N-S)	25.29	25.29	0.04	1.00	0.97	7.1
6	Bending (E-W)	36.09	36.10	0.03	1.00	0.91	6.5
7	Torsion	40.73	40.73	0.03	1.00	0.86	4.6
8	Bending (N-S)	40.78	40.82	0.03	1.00	1.09	5.5
9	Bending (E-W)	46.27	46.28	0.03	1.00	1.03	5.1
10	Bending (N-S)	55.50	55.47	0.03	1.00	0.97	6.0
11	Torsion	62.52	62.49	0.02	1.00	0.95	2.6
12	Torsion	80.80	80.83	0.02	1.00	0.98	3.3

Figure 3.7, Figure 3.8, and Figure 3.9 illustrate the estimated mode shapes for the simulated benchmark problem. The dashed lines in these three dimensional plots represent the undeformed configuration of the structure, whereas the solid lines correspond to the deformed shape for each mode. The associated frequency and modal damping ratio are also given above each plot.

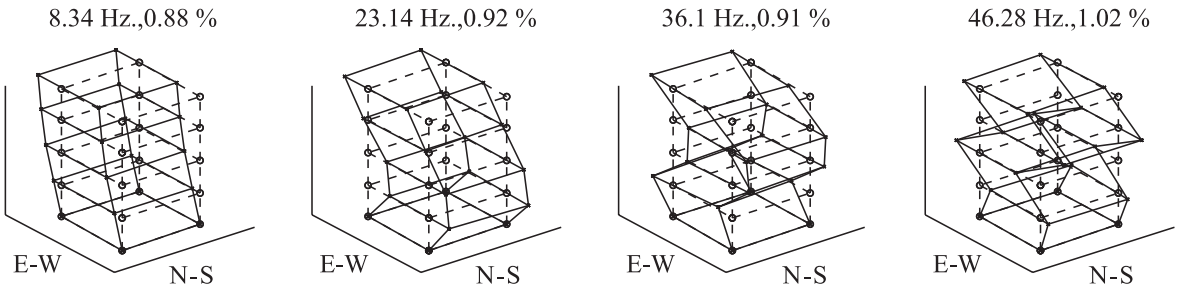

Figure 3.7. Estimated bending mode shapes along E-W direction for the Phase II analytical benchmark problem

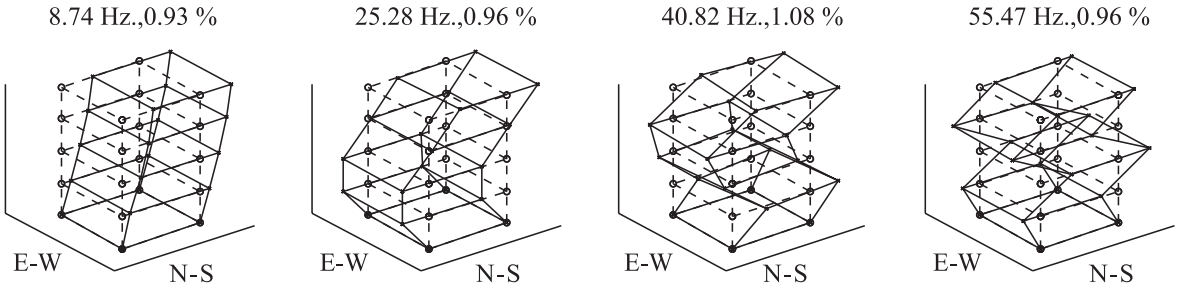

Figure 3.8. Estimated bending mode shapes along N-S direction for the Phase II analytical benchmark problem

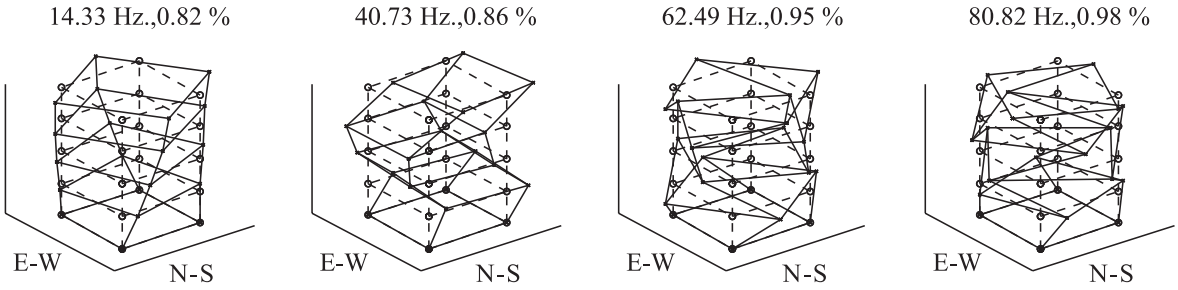

Figure 3.9. Estimated torsional mode shapes for the Phase II analytical benchmark problem

A remark should be added at this point of the discussion regarding the classical damping assumption implicitly made while estimating the tabulated modal parameters. In this part of the study there exists no concern about their validity since data is already simulated from a classically damped system. While working with real life data, on the other hand, this assumption needs to be substantiated. For this purpose, a criterion called Modal Phase Collinearity (MPC) will be used. This criterion was formulated by Juang and Pappa (1985) to help interpret the analysis results obtained by ERA.

The MPC begins with the idea of a monophase mode. A monophase mode is the one that has the same phase at all spatial output points. This means, for instance, that each output reaches its respective maximum displacement at the same time while vibrating in that mode. Theoretically, the mode vectors of a classically damped system will exhibit monophasicity since the modal vectors are expected to be real in this case. The motivation behind MPC is to scale a complex mode vector such that the resulting vector is as close to real as possible, and then quantify the complex residuals to give a measure of how close the vector is to monophase behavior.

The derivation of the MPC follows the one presented by Tolson (1991). Consider first the identified m dimensional complex modal vector ψ

$$\psi = \begin{bmatrix} a_1 + jb_1 \\ a_2 + jb_2 \\ \vdots \\ a_m + jb_m \end{bmatrix} = \begin{bmatrix} r_1 e^{j\theta_1} \\ r_2 e^{j\theta_2} \\ \vdots \\ r_m e^{j\theta_m} \end{bmatrix} \tag{3.4}$$

where a_i and b_i denote the real and imaginary parts, and r_i and θ_i represent the absolute value and phase angle of each component. Let θ be the angle that makes ψ real such that

$$\bar{\psi} = \psi e^{j\theta} \tag{3.5}$$

where $\bar{\psi}$ is a real vector. $\bar{\psi}$ may not be exactly real due to the noise in the data, but it is possible to minimize the imaginary parts in a mean square sense. Therefore the problem can be stated more precisely as finding the angle θ that minimizes the sum of the squares of the complex parts as

$$J = \sum_{i=1}^{m} \left[\mathrm{Im}\left(r_i e^{j(\theta_i + \theta)} \right) \right]^2 \tag{3.6}$$

This minimization problem can be solved by forcing $\frac{\partial J}{\partial \theta} = 0$ which yields

$$\tan 2\theta = \frac{2\sum_{i=1}^{m} a_i b_i}{\sum_{i=1}^{m}\left(b_i^2 - a_i^2\right)} \tag{3.7}$$

and, using Eq. (3.7) a measure of deviation for the imaginary residues can be computed which reads

$$J = \sum_{i=1}^{m}\left[b_i^2 + \left(a_i^2 - b_i^2\right)\sin^2\theta + a_i b_i \sin 2\theta\right] \tag{3.8}$$

The MPC is then defined as

$$MPC = 1 - \frac{J}{\sum_{i=1}^{m} a_i^2 + \sum_{i=1}^{m} b_i^2} \tag{3.9}$$

and has a range between 0 and 1, where 0 indicates a mode with no phase coherence and 1 means a normal mode.

Table 3.4. MPC values for the Phase II analytical benchmark problem

Mode #	Type	ω (Hz)	ζ (%)	MPC (%)
1	Bending (E-W)	8.35	0.88	99.8
2	Bending (N-S)	8.74	0.93	99.7
3	Torsion	14.34	0.82	93.8
4	Bending (E-W)	23.15	0.92	100.0
5	Bending (N-S)	25.29	0.97	100.0
6	Bending (E-W)	36.09	0.91	100.0
7	Torsion	40.73	0.86	77.8
8	Bending (N-S)	40.78	1.09	93.1
9	Bending (E-W)	46.27	1.03	100.0
10	Bending (N-S)	55.50	0.97	100.0
11	Torsion	62.52	0.95	99.3
12	Torsion	80.80	0.98	98.9

Table 3.4 presents the MPC values corresponding to the identified mode shapes for the analytical benchmark problem. The lowest values are associated with the two closely

spaced modes around 40.7 Hz. The corresponding mode shape plots also confirm this indication because the deformed patterns of these two modes look almost identical and it seems as if the torsional motion has not been properly uncoupled from the bending mode. Pappa et al. (1993) indeed point out that significant phase angle errors can occur for closely spaced modes when the excitation is inadequate to uncouple these modes, and this might be a possible explanation for the low MPC values concerning these two modes.

3.2.2. Experimental Phase

In the experimental phase of the benchmark problem, the model structure shown in Figure 3.4 is instrumented with three uniaxial accelerometers at each story level including the base. Two of these measure the N-S motion and the remaining one is placed near the center column to measure the E-W (Figure 3.10). As for the excitation, the structure is subjected to ambient loads due to wind, pedestrians and traffic. The sampling rate is 200 Hz, and the test duration is 300 seconds. A detailed description of the test structure and experimental procedure can be found on the ASCE SHM website, and is also discussed by Dyke et al. (2003).

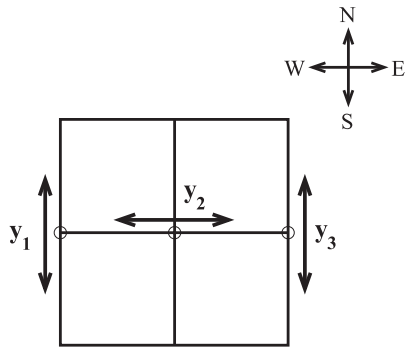

Figure 3.10. Measurement setup for the Phase II experimental benchmark problem

Before proceeding with the modal analysis, the data is detrended in order to remove the mean and drift due to sensor inaccuracies. The base accelerations are excluded and thus the total number of output channels is 12. The first 10 seconds of measurements are not considered in the analysis, and the remaining time histories are divided into three non-overlapping segments. These three segments are then analyzed separately, and the results

which are obtained mutually from all three data sets are considered to qualify as system modes.

Initially, a 480 state model is constructed using the CVA weighted SSI-DATA algorithm. In the reduction step this higher order model is reduced to $n = 2,3,...,300$, and the corresponding modal parameters are estimated for each order. The stabilization diagrams for all three data sets are given in Figure 3.11, Figure 3.12, and Figure 3.13 to aid visual judgment of the stable modes. The criteria for modal parameter discrepancies are set to be $\rho_{\omega} = 1\%$, $\rho_{\zeta} = 4\%$ and $\rho_{MAC} = 1\%$ in these diagrams, and again the continuous line represents the PSD estimate of the output. There are seven modes that appear consistently in all three analyses. In addition, these plots suggest that there exists a high modal density in the 25-30 Hz. frequency range which may interrupt proper identification of any modes located herein.

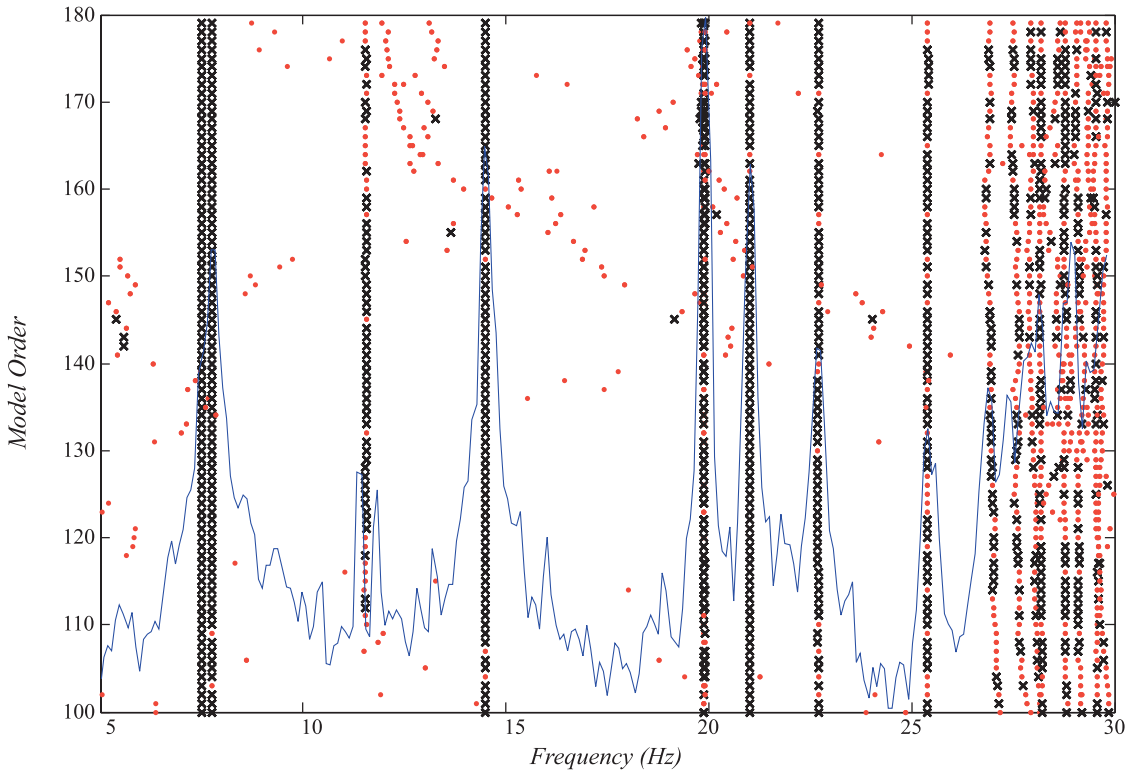

Figure 3.11. Stabilization diagram for the Phase II experimental benchmark problem (First time history)

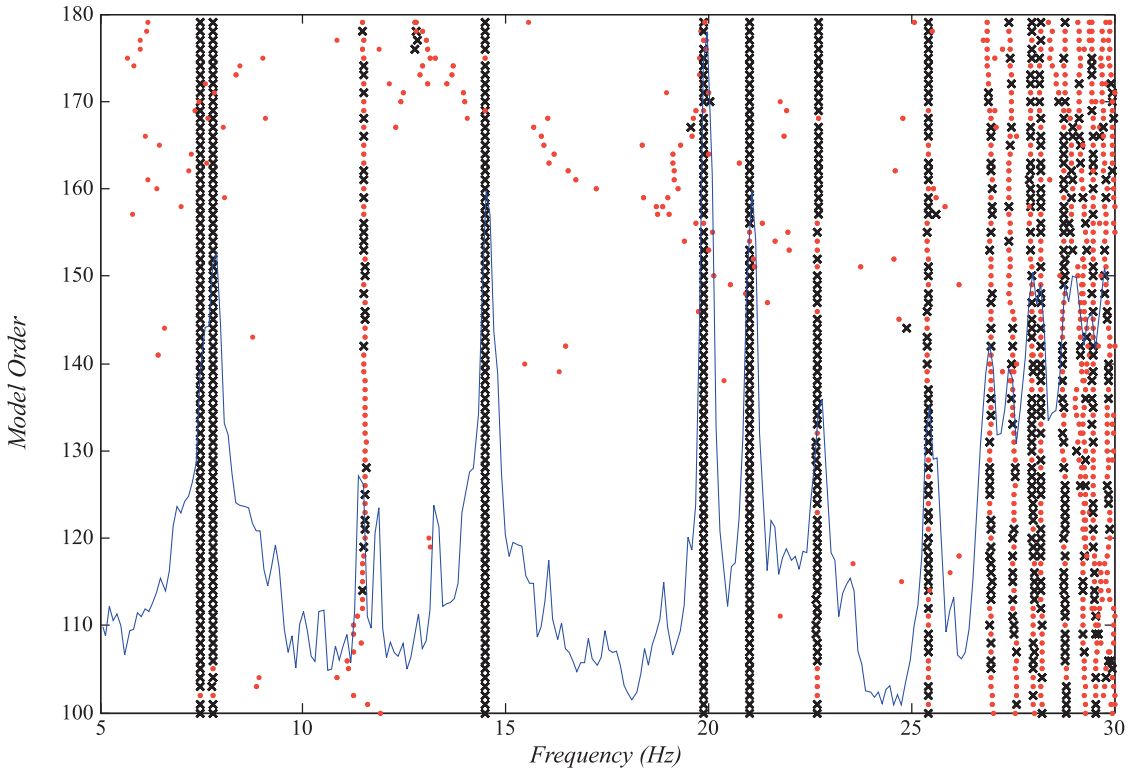

Figure 3.12. Stabilization diagram for the Phase II experimental benchmark problem (Second time history)

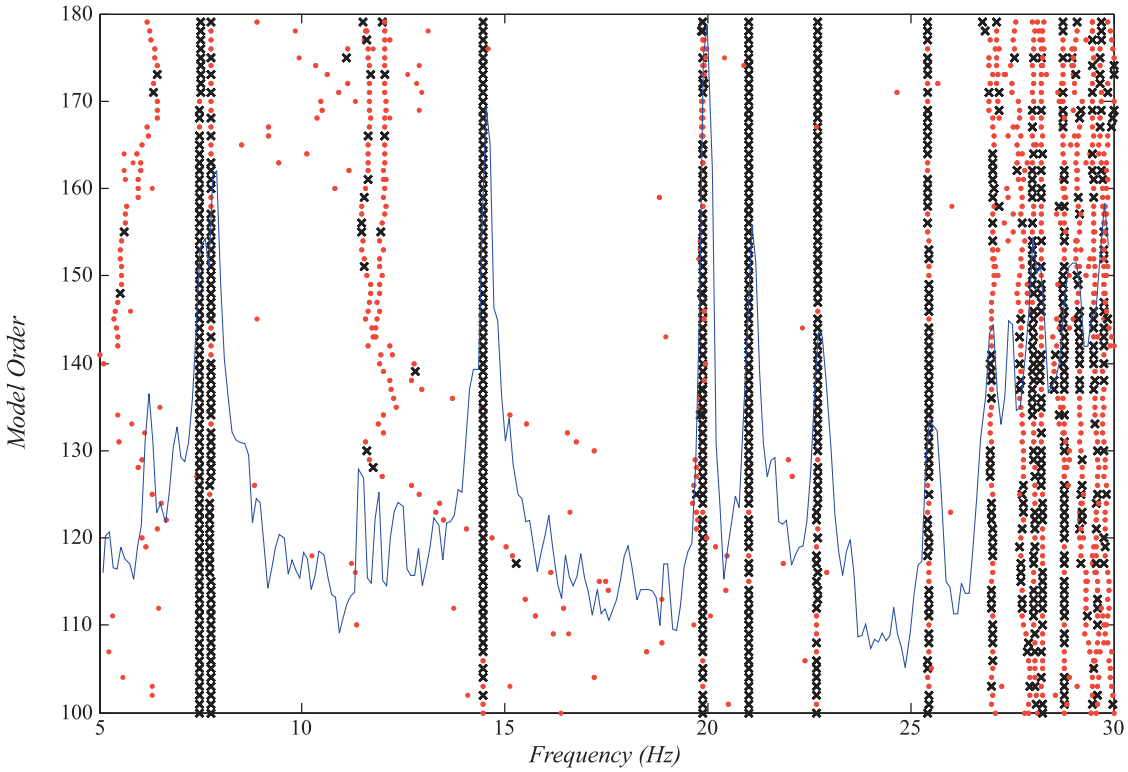

Figure 3.13. Stabilization diagram for the Phase II experimental benchmark problem (Third time history)

The identified modal parameters are clustered using $\Delta_{\omega} = 0.5\%$, $\Delta_{\zeta} = 0.05\%$, $\Delta_{MAC} = 0.01$ and $\tau = 1$, but using all the available sets of modal parameters instead of the refined results obtained in the initial stabilization diagram step.

Table 3.5. Clustering analysis results for the Phase II experimental benchmark problem

Mode #	Type	ω (Hz)		ζ (%)		MPC
		Mean	δ (%)	Mean	δ (%)	
1	Bending (E-W)	7.49	0.08	0.67	9.79	95.8
2	Bending (N-S)	7.76	0.09	0.69	15.41	96.3
3	Torsion	14.48	0.03	0.15	55.34	94.6
4	Bending (E-W)	19.89	0.00	0.00	194.32	92.8
5	Bending (N-S)	21.01	0.02	0.07	74.90	81.4
6	-	22.70	0.04	0.45	12.61	25.2
7	Bending (E-W)	25.41	0.04	0.21	33.33	90.0
8	Bending (E-W)	28.19	0.04	0.18	21.00	86.2

Table 3.5 presents the summary of the results pertaining to modal parameters identified consistently in all three data sets. The MPC values are also given to assess the validity of the classical damping assumption. The estimated mode shapes illustrated in Figure 3.14 suggest that there exists coupling between translational motions to some extent due probably to the eccentric placement of the floor masses; hence the classification of the modes as given in Table 3.5 is based on the most dominant direction of motion for that mode.

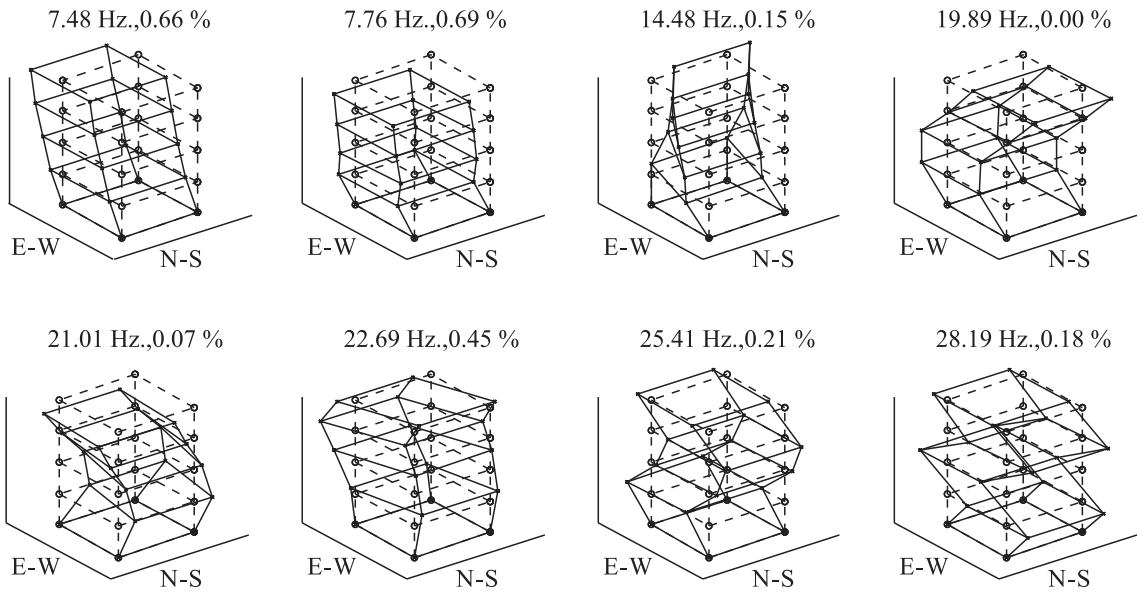

Figure 3.14. Estimated mode shapes for the Phase II experimental benchmark problem

One of the noteworthy results is the negligibly small modal damping ratio associated with the second bending mode identified along E-W direction. Although the MPC value and the associated mode shape plot seem to be satisfactory for this mode, the zero damping ratio suggests some kind of trouble. The second remark concerns the sixth identified mode that has a natural frequency of 22.7 Hz. For this mode, the MPC value does not appear to be acceptable even though it has been identified with good consistency in all three data sets.

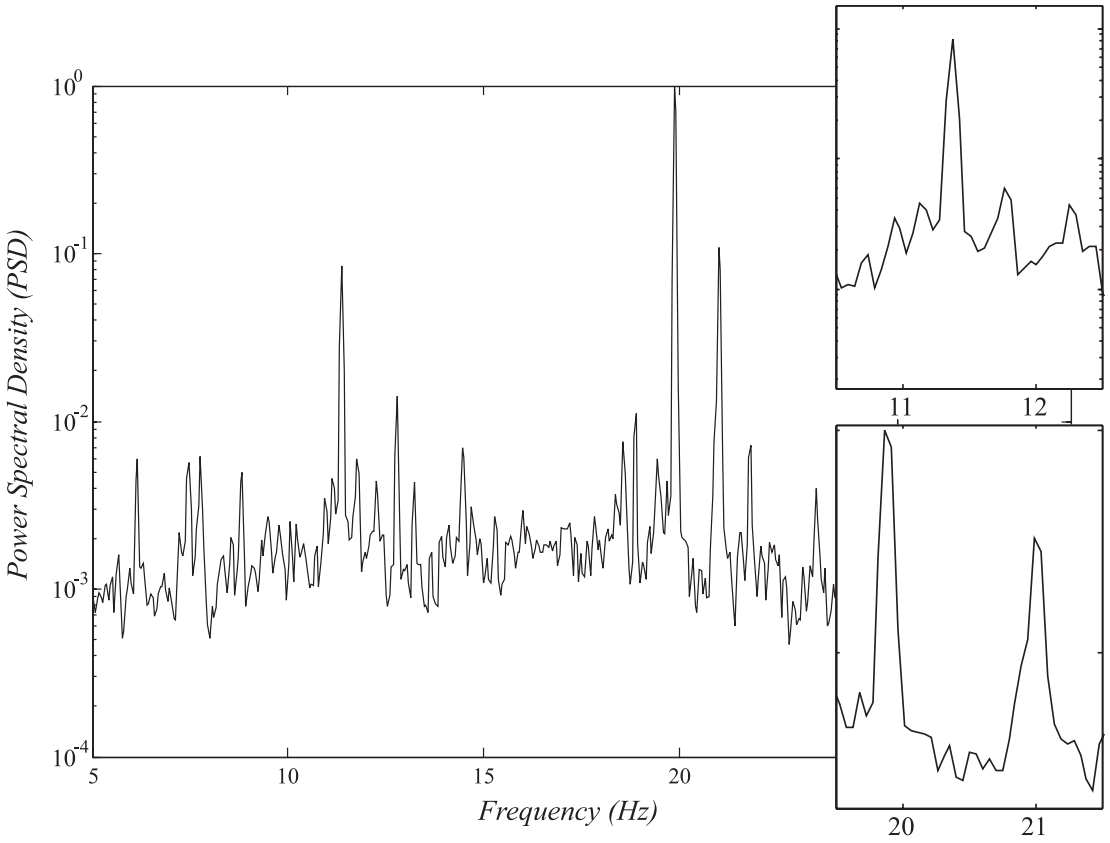

Figure 3.15. Power spectral density estimate of the acceleration signals measured at the base level

Figure 3.15 shows the power spectral density plot of the acceleration measurements recorded at the base level. The two zooms reveal three frequencies (11.3 Hz., 19.9 Hz. and 21 Hz.) around which there is a considerable amount of energy accumulation. As far as the base is properly fixed, there should not be any dominant frequency components in these signals. Assuming that there is no such violation of the fixed support conditions, these frequency components might be attributed to some harmonic excitation present in the

environment. If this claim is correct, the identified fourth and fifth modes can no more be considered as system modes.

This problem was also studied by Ching and Beck (2003) with a two-stage Bayesian SHM approach, and some of their results are presented in Table 3.6 in order to facilitate a comparison basis for the SSI results.

Table 3.6. Modal parameters for the Phase II experimental benchmark problem by Ching and Beck (2003)

Mode #	Type	ω (Hz)	ζ (%)
1	Bending (E-W)	7.48	0.60
2	Bending (N-S)	7.76	0.37
3	Torsion	14.48	0.06
4	Bending (E-W)	19.89	0.01
5	Bending (N-S)	21.01	0.01

3.3. Vincent Thomas Suspension Bridge

The final analysis in this study investigates the performance of the SSI methodology with regards to modal parameter identification of large scale structures. The structure considered for this purpose is the Vincent Thomas Suspension Bridge (Figure 3.16) located in Los Angeles, California. The bridge has of a main span of length 457.2 m and two side spans of length 154.5 m each. The deck is 16 m wide steel truss with lateral K-bracing that provide torsional stiffness. The main span is supported by two towers, each 120 m tall, which rest on steel piles.

The bridge is instrumented with 26 uniaxial strong ground motion sensors since mid 1980s as a part of the California Strong Motion Instrumentation Program. The deployment of the sensors is shown in Figure 3.17. Here we only use the acceleration measurements obtained from the 16 stations located on the superstructure, and exclude also station 4 which malfunctioned during the test. The data is sampled at a frequency of 100 Hz, and the measurements constitute a total duration of one hour yielding 360000 output samples per channel.

Figure 3.16. Photograph of the Vincent Thomas Bridge (Pridham and Wilson, 2002)

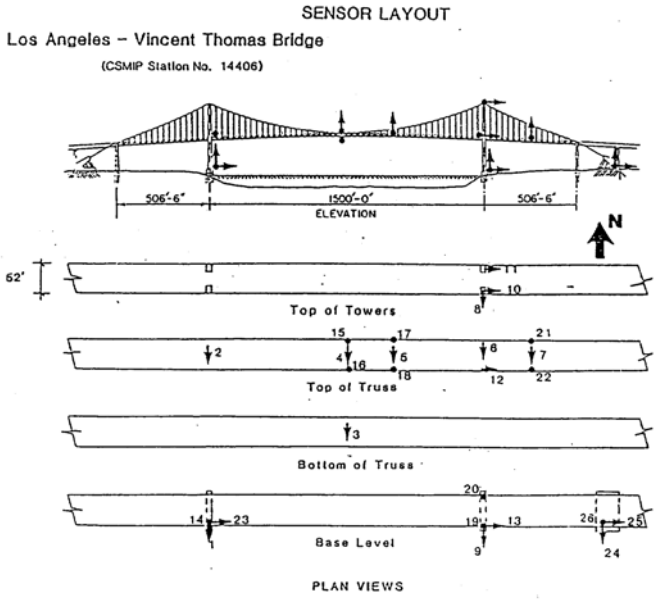

Figure 3.17. Sensor setup on the Vincent Thomas Suspension Bridge (Abdel-Ghaffar and Masri, 1992)

Before using the output measurements in the identification algorithms, it is sometimes important to consider some measures to make the data easy to handle. Two data preprocessing tools that are useful in this context are filtering and decimation.

If the frequency range of interest can be anticipated beforehand, a suitable filter can be utilized to remove the undesired frequency components from the data. Depending on the range of interest, these undesired components might be the lower or higher frequencies, or

some combination of both. The filters to be considered in each of these cases are highpass, lowpass and bandpass filters, respectively.

If the measured data is sampled at a very high sampling frequency compared to the anticipated frequency range of interest, then it is advisable to decimate the data by some appropriate factor to improve numerical accuracy and better concentrate on the desired frequencies (McKelvey, 1995). Decimation is simply resampling the data at a lower frequency, but a filtering should be always applied before this operation in order to avoid folding of frequencies.

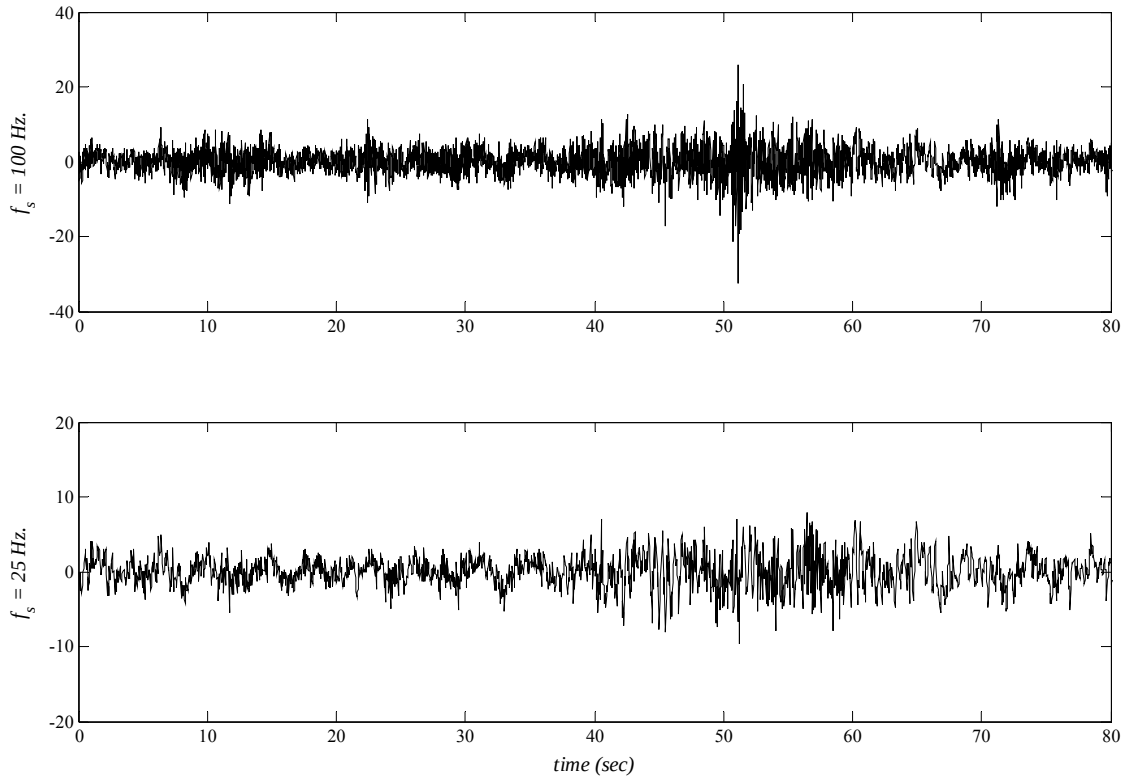

Figure 3.18. Acceleration measurements from channel 15 before and after resampling at a frequency of 25 Hz.

Going back to the Vincent Thomas Suspension Bridge, the initial step of the analysis is to detrend the data to remove the mean and drift that might adversely affect the results. This is followed by the decimation step where the original sampling frequency has been reduced by a factor of four after applying a Chebyshev Type I lowpass filter with a normalized cutoff frequency of 10 Hz. This operation reduces the sampling frequency to 25 Hz. Figure 3.18 shows a segment of the acceleration response obtained from channel 15

both before and after data preprocessing. The effect of the removal of higher frequency components is apparent in the second plot in that the lower frequency waves can be distinguished more visibly.

As for the modal identification analysis, the CVA weighted SSI-DATA algorithm is utilized to initially construct a model with 1800 states. Realizing such a high order model using all the available output samples is not possible due to computational limitations so a time history that depicts relatively stationary behavior for a total duration of 400 seconds is considered for the following analysis. The initial higher order model is reduced to $n = 400, 401, ..., 600$, and the associated modal parameters are clustered using $\Delta_\omega = 0.5\%$, $\Delta_\zeta = 0.05\%$, $\Delta_{MAC} = 0.01$ and $\tau = 1$. A stabilization diagram is also generated as a visual aid (Figure 3.19) with respective tolerances $\rho_\omega = 1\%$, $\rho_\zeta = 4\%$. Note that the system order has to be increased substantially in order to obtain satisfactory results even though the sampling frequency is decreased by a factor of 4.

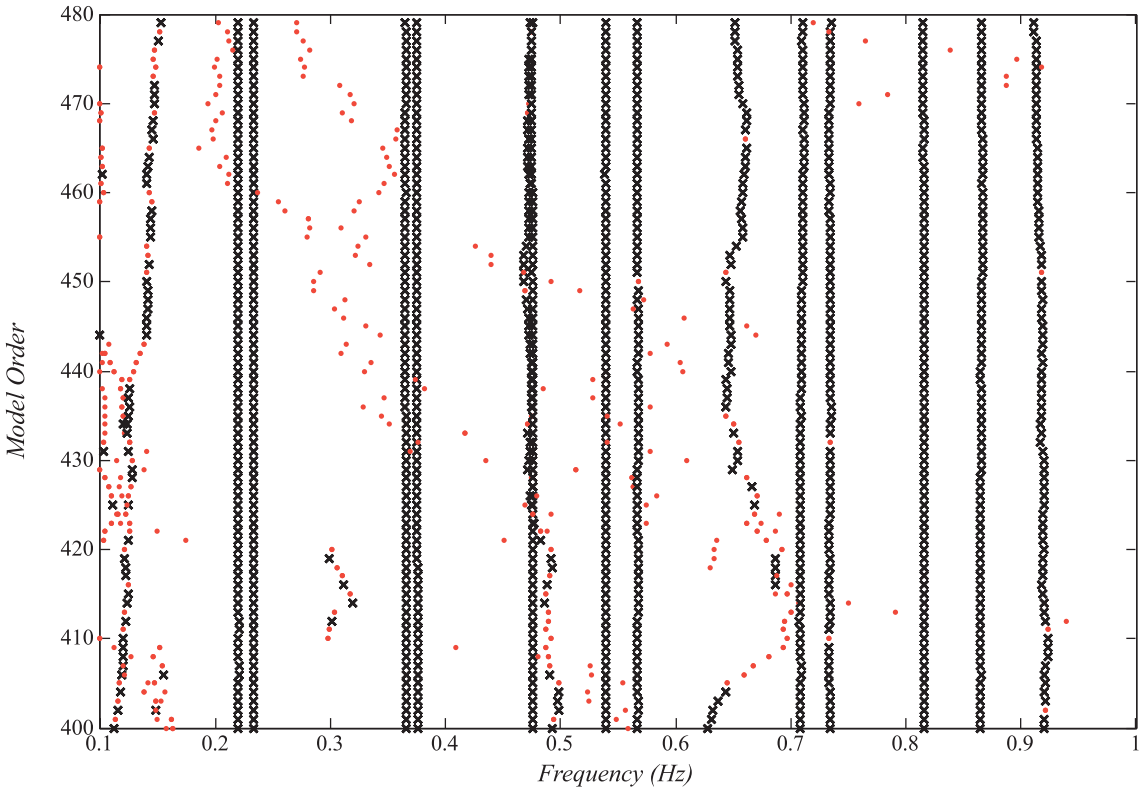

Figure 3.19. Stabilization diagram for the Vincent Thomas Bridge ($f_s = 25Hz$)

For such a lightweight and slender structure as the Vincent Thomas Bridge the fundamental frequencies are expected to lie below 1 Hz, and furthermore the sensor setup on the bridge is not dense enough to reliably visualize the multi-noded mode shapes that belong to higher frequencies. The present analysis, therefore, focuses mainly on the frequency range 0-1 Hz. Table 3.7 presents a summary of the clustering analysis results, and the corresponding mode shapes are plotted in Figure 3.20.

Table 3.7. Modal parameter estimates for the Vincent Thomas Bridge ($f_s = 25Hz$)

Mode #	Type	ω (Hz)		ζ (%)		MPC
		Mean	δ (%)	Mean	δ (%)	
1	Vertical	0.219	0.09	3.1	3.08	90.3
2	Vertical	0.232	0.05	2.3	6.12	95.1
3	Vertical	0.365	0.08	1.9	5.33	99.0
4	Vertical	0.375	0.05	1.6	6.37	99.2
5	Vertical	0.475	0.03	1.4	7.90	99.8
6	Torsional	0.538	0.05	0.9	9.05	99.4
7	Vertical	0.567	0.03	0.7	5.52	99.9
8	-	0.705	0.08	1.7	1.71	80.3
9	Torsional	0.734	0.06	1.9	6.28	95.6
10	Vertical	0.815	0.01	0.6	1.05	99.2
11	-	0.864	0.05	1.9	4.75	93.0
12	-	0.911	0.15	3.5	3.85	88.0

The classification of the bridge vibration modes as given in Table 3.7 is based on the description made by Abdel-Ghaffar and Housner (1977). In pure vertical modes, all points on any cross section of the bridge move vertically with equal displacements, and remain in phase. Torsional motion involves the rotation of the cross sections about the longitudinal axis of the bridge. Finally, in pure lateral modes a sway motion is observed in which each cross section swings like a pendulum in its own vertical cross section. As can be seen from Table 3.7 and Figure 3.20, some fundamental vertical and torsional modes have been figured out with satisfactory consistency indicators (i.e., the density of the clusters and the MPC values). However, no pure lateral modes have been identified in this analysis. This might be attributed to the insufficient excitation of these modes during the test (or specifically during the time window considered).

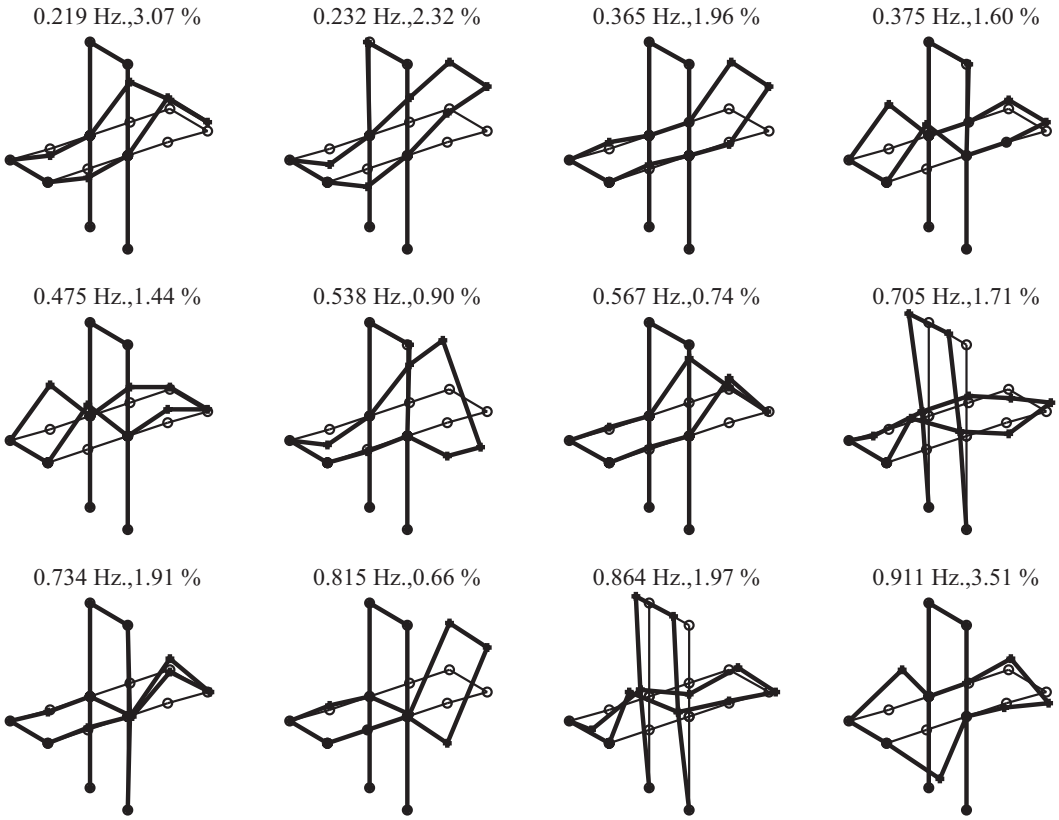

Figure 3.20. Estimated mode shapes of the Vincent Thomas Bridge ($f_s = 25Hz$)

In order to further appreciate the effects of preprocessing techniques on the identification accuracy, another analysis has been undertaken where the data is decimated by a factor of 20 this time. Prior to decimation, the higher frequency components in the data are removed using a Chebyshev Type I lowpass filter with a normalized cutoff frequency of 2 Hz. The new sampling frequency is 5 Hz. A representative time history window from the acceleration responses measured at channel 15 both before and after decimation are given in Figure 3.21. The contributions of the lower frequencies to the response are more prominent in this figure as compared to Figure 3.18.

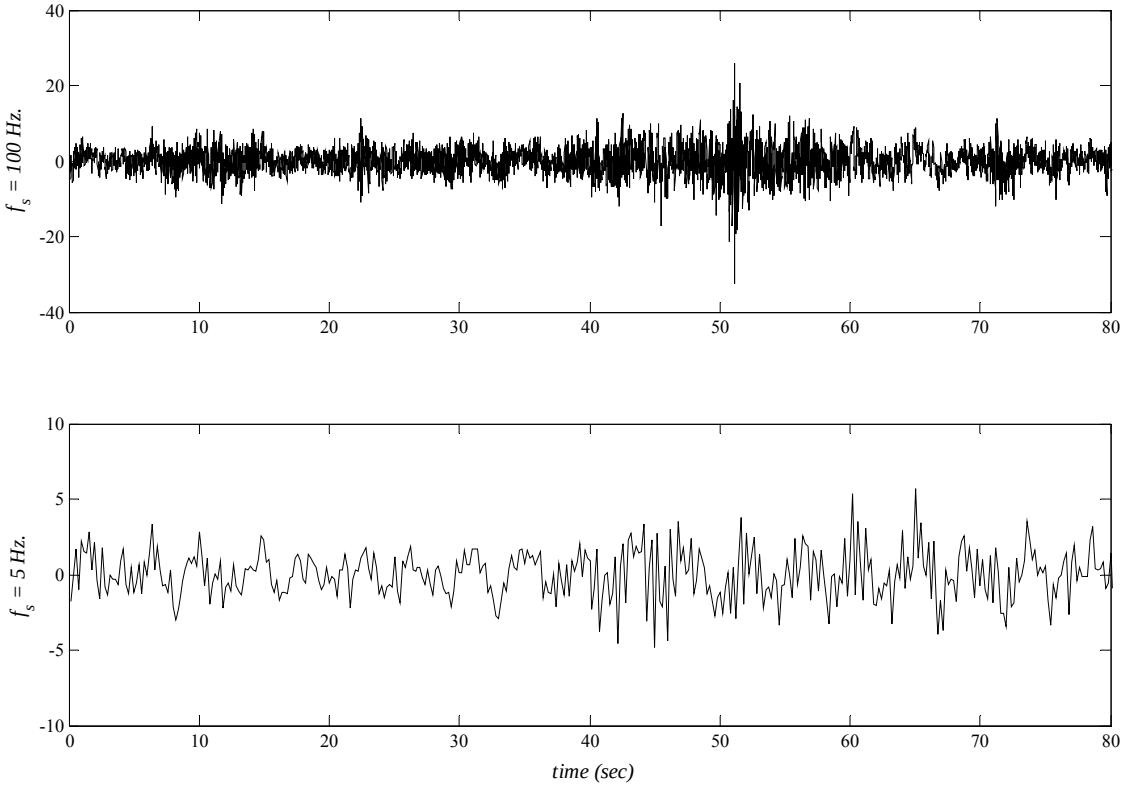

Figure 3.21. Acceleration measurements from channel 15 before and after resampling at a frequency of 5 Hz.

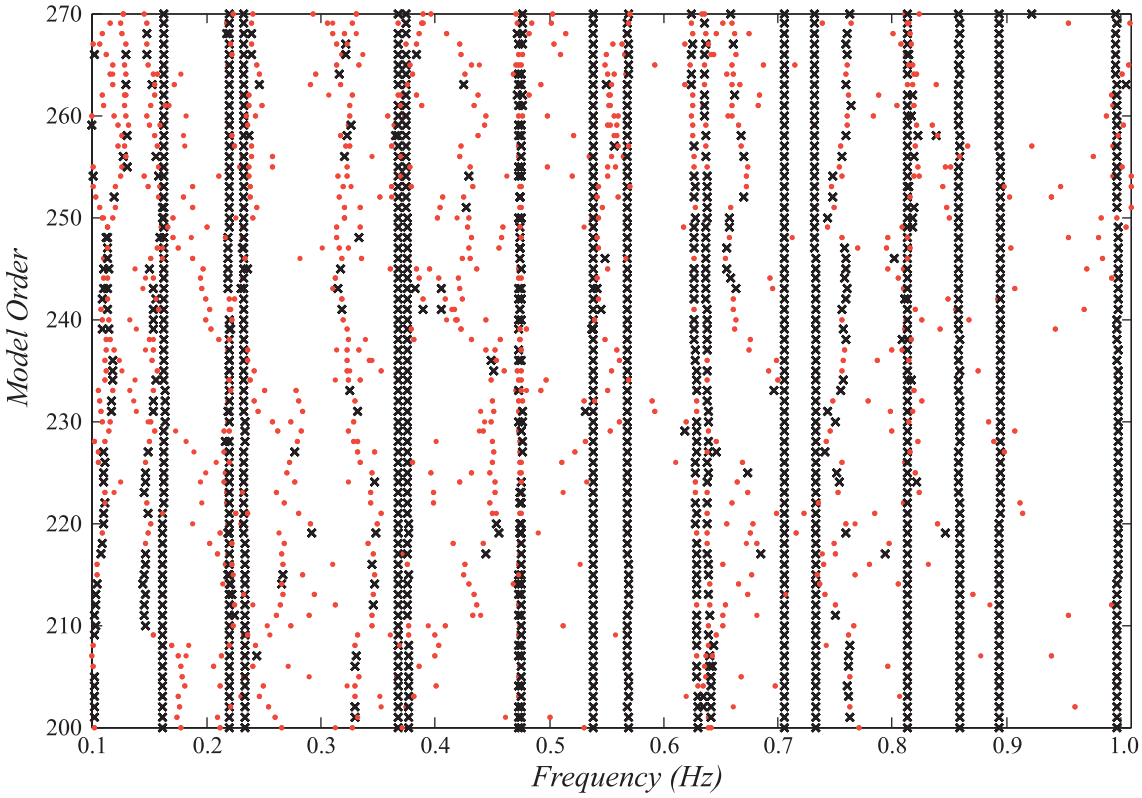

Figure 3.22. Stabilization diagram for the Vincent Thomas Bridge ($f_s = 5Hz$)

In this second analysis, the initially realized model has 600 states, and since there is no computational complexity involved in identifying a model of this order using 18000 samples, all the available output measurements are employed in the SSI-DATA (CVA) algorithm. This 600 state model is then reduced to $n = 200, 201, \ldots 400$ which are significantly less demanding in terms of computation time compared to the orders used in the previous analysis. The rest of the analysis is exactly the same as the previous one. The associated stabilization diagram is shown in Figure 3.22, and the clustering analysis results are summarized in Table 3.8.

Table 3.8. Modal parameter estimates for the Vincent Thomas Bridge ($f_s = 5Hz$)

Mode #	Type	ω (Hz)		ζ (%)		MPC
		Mean	δ (%)	Mean	δ (%)	
1	-	0.162	0.27	4.2	5.35	60.1
2	Vertical	0.220	0.06	1.5	4.82	99.7
3	Vertical	0.233	0.11	1.3	8.00	99.9
4	Vertical	0.368	0.04	1.1	3.42	92.6
5	Vertical	0.375	0.18	2.2	8.14	99.5
6	Vertical	0.475	0.09	1.6	7.94	93.9
7	Torsional	0.539	0.03	0.6	5.22	99.6
8	Vertical	0.569	0.03	1.1	4.37	99.0
9	-	0.706	0.04	0.5	5.72	87.5
10	Torsional	0.732	0.12	1.3	9.99	98.8
11	Vertical	0.814	0.11	0.8	8.58	99.9
12	-	0.859	0.02	1.0	3.80	89.1
13	-	0.895	0.09	1.7	7.73	97.2
14	-	0.997	0.07	1.1	5.75	96.5

Both the stabilization diagram and the tabulated results suggest that there are 14 modes located in the 0-1 Hz. frequency interval which consistently appear in all of the identified lower order models. The most notable difference in between the two analyses is the mode with 0.162 Hz. frequency. This mode has not been identified in the first analysis, but here it appears to be one of the most “stable” modes. The associated modal damping ratio is in the order of magnitudes that are acceptable for a lightweight and slender structure. It is hard, on the other hand, to classify this mode as a pure vertical, torsional or lateral one based on the rather odd mode shape shown in Figure 3.23. Although it seems to be dominated by both vertical and lateral motion, this conclusion should be read with great care considering the related MPC value (60.1 %).

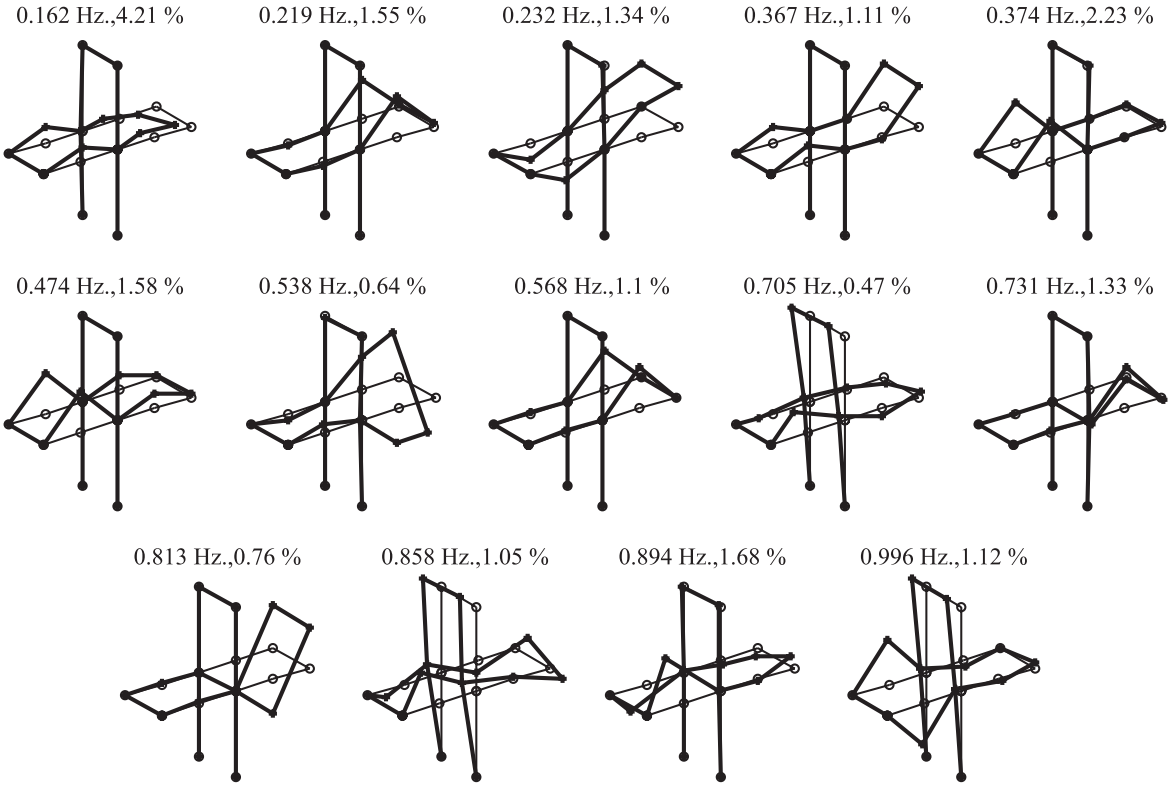

Figure 3.23. Estimated mode shapes for the Vincent Thomas Bridge ($f_s = 5Hz$)

Table 3.9. Comparison of modal parameters obtained from two different analyses

Analysis #1 ($f_s = 25Hz$)		Analysis #2 ($f_s = 5Hz$)		MAC(%)
ω (Hz)	ζ (%)	ω (Hz)	ζ (%)	
-	-	0.162	4.2	-
0.219	3.1	0.220	1.5	93.9
0.232	2.3	0.233	1.3	98.4
0.365	1.9	0.368	1.1	90.3
0.375	1.6	0.375	2.2	98.6
0.475	1.4	0.475	1.6	98.6
0.538	0.9	0.539	0.6	96.0
0.567	0.7	0.569	1.1	99.6
0.705	1.7	0.706	0.5	92.9
0.734	1.9	0.732	1.3	97.5
0.815	0.6	0.814	0.8	99.7
-	-	0.859	1.0	-
0.864	1.9	-	-	-
-	-	0.895	1.7	-
0.911	3.5	-	-	-
-	-	0.997	1.1	-

Even though some differences are observed between the results of the two analyses, some of the identified modes agree well with each other in both cases. Table 3.9 presents the results pertaining to both analyses on a comparative basis such that the modes that have close modal frequency and damping ratio estimates are tabulated side by side. The MAC values are also evaluated to further assess the degree of correlation in between these modes. Except for three values, they are all above 96% which suggests a satisfactory correspondence for the estimated mode shapes.

The ambient vibration measurements of this bridge have been studied by various researchers applying different system identification techniques. Abdel-Ghaffar and Housner (1978) have used the more classical peak picking method. The more recent studies involve the application of the SSI-COV algorithm by Luş et al. (2004), and Pridham and Wilson (2002). Some of the results obtained by Abdel-Ghaffar and Housner are presented in Table 3.10 for comparison purposes.

Table 3.10. Modal parameters for the Vincent Thomas Bridge by Abdel-Ghaffar and Housner (1978)

Mode #	Type	ω (Hz)	ζ (%)
1	Lateral	0.168	2.0 ~ 2.8
2	Vertical	0.216	1.4 ~ 1.8
3	Vertical	0.234	2.1 ~ 2.3
4	Vertical	0.366	0.7 ~ 1.1
5	Vertical	0.385	1.0 ~ 1.5
6	Vertical	0.487	0.8 ~ 1.0
7	Torsional	0.494	0.7 ~ 0.9
8	Lateral	0.542	0.9 ~ 1.0
9	Vertical	0.579	0.5 ~ 0.6
10	Lateral	0.623	0.4 ~ 0.5
11	Lateral	0.678	-
12	Torsional	0.740	0.5 ~ 0.7
13	Torsional	0.806	0.4 ~ 0.6
14	Vertical	0.835	0.7 ~ 0.9
15	Lateral	0.879	0.4 ~ 0.6
16	Torsional	0.945	0.4 ~ 0.5

4. CONCLUSIONS

The aim of this study was to assess the comparative merits of different stochastic subspace identification algorithms, and investigate their use for modal analysis of some structures to find out what the potential benefits and pitfalls are.

The results of the Monte Carlo simulation discussed in Section 3.1 revealed that the performances of the covariance and data driven subspace algorithms are similar as far as the accuracy of the identified modal parameters are concerned. This finding was indeed implied in the discussion pertaining to the implementation details of these algorithms. Though the analytical relations have not been established, the data projection step involved in the data-driven algorithm appears to be a notion similar to the explicit computations of the output covariances. By estimating covariances, one obtains a free decay response in some sense. The projection operation aims, on the other hand, at obtaining an improved estimate of some partition of the available data based on the remaining partition, thereby removing the contributions of the uncorrelated modes to the improved partition.

The main distinction seems to occur due to the realization basis used in both algorithms. The Canonical Variate Analysis approach has been found to perform superior when compared with the Balanced Realization weighting. As is evident from the derivation of the covariance-driven algorithm, Canonical Variate Analysis basically weights the output covariances with some other output covariance estimates. In this manner, it might be dampening out noise modes while revealing the effects of the actual system modes on the derived free decay responses. Finally, it has been observed that the damping estimates are usually identified with much less accuracy than the frequencies and mode shapes.

In real life engineering structures, the fundamental problem is the determination of the system order or, in other words, differentiating true structural modes from spurious noise modes. Two different approaches were considered in this study, both of which are indeed based on the same motivation: System modes are expected to appear consistently in a set of identified models of different orders whereas the spurious ones are expected to show a somewhat more erratic behavior. The stabilization diagrams proved to be useful

tools for visually judging the number of significant modes. The main drawback about this approach is the large amount of user interaction required for this judgment process. Although it is possible to automate the mode selection process, there might be some algorithmic complications due to the order wise sequential construction of these diagrams. The clustering analysis, on the other hand, automates the grouping of these stable modes in a more reliable way, i.e. the computer looks at the data instead of the user and selects the modes that show consistency at sufficiently many system orders. In order to enforce a computer to make such a decision, it is inevitable to define some threshold values, and the analysis results become quite sensitive to these predefined thresholds in return. Many trials and errors might be necessary to achieve a satisfactory result with the clustering analysis, and this, in fact, constitutes the basic tradeoff between automation and user interaction. On the whole, both of these approaches can be criticized as being more heuristic than mathematically robust, and a reliable and computationally less demanding way of determining the system order is still an open problem.

The second major issue discussed here was the validity of the classical damping assumption for the identified modal parameters. How 'classical' a mode is depends on the relative phase differences of its components, so that validation can be done by simply looking at the phase angles of the components of a vector. If the phase angles are spaced 0 or π rads apart for a specific complex mode vector, then it might be claimed that this mode vector defines a monophase behavior. The phase angles, however, are much more sensitive to noise than the relative magnitudes, such that a component which has a very small effect on the deformation shape may require a big penalty because of the large deviation in its phase angle. In general, therefore, an interpretation base solely on the phase angle information may be misleading. In this respect, the Modal Phase Collinearity has been found to be a practically useful accuracy indicator that can be used to properly discuss the monophase behavior. The basic rationale behind this parameter is to try to scale a complex modal vector such that the complex parts are minimized. The remaining complex residuals are then normalized with respect to a value that is invariant under the above transformation, and this normalized value suggests the degree of justification for the classical damping assumption. The implications of this parameter in the applications involving experimental data analysis were indeed quite reasonable.

The experiences with the experimental data have shown that the SSI algorithms perform quite satisfactorily and provide a well defined framework for ambient data analysis. On the other hand, a large amount of pre-processing of data might be required depending on the sampling process and the complexity of the structure. To this end, preprocessing tools such as filtering and decimation have been found to be useful in reducing the computational burden and improving the results of the identification. These benefits were most evident in the analysis of the Vincent Thomas Bridge wherein the pre-processing helped to focus on the fundamental frequencies of this large scale structure which were extremely difficult to detect properly without preconditioning.

REFERENCES

Abdel-Ghaffar, A. M. and G. W. Housner, 1977, *An Analysis of the Dynamic Characteristics of a Suspension Bridge by Ambient Vibration Measurements*, Report EERL 77-01, Earthquake Engineering Research Laboratory, California Institute of Technology.

Abdel-Ghaffar, A. M. and G. W. Housner, 1978, "Ambient Vibration Tests of Suspension Bridge", *Journal of the Engineering Mechanics Division*, Vol. 104, No. 5, pp. 983-999.

Abdel-Ghaffar, A. M. and S. F. Masri, 1992, "Seismic Performance Evaluation of Suspension Bridges", *Proceedings of the 10th World Conference on Earthquake Engineering*, Rotterdam, pp. 4845-4850.

Akaike, H., 1974, "Stochastic Theory of Minimal Realization", *IEEE Transactions on Automatic Control*, Vol. AC-19, No. 6, pp. 667-674.

Akaike, H., 1975, "Markovian Representation of Stochastic Processes by Canonical Variables", *Siam Journal on Control and Optimization*, Vol. 13, No. 1, pp. 162-173.

Andersen, P., 1997, *Identification of Civil Engineering Structures Using Vector ARMA Models*, Ph.D. Dissertation, Department of Civil Engineering, K. U. Leuven, Belgium.

Arun, K. S. and S. Y. Kung, 1990, "Balanced Approximation of Stochastic Systems" *Siam Journal on Matrix Analysis and Applications*, Vol. 11, No. 1, pp. 42-68.

ASCE SHM benchmark website, 2006,
http://cive.seas.wustl.edu/wusceel/asce.shm/benchmarks.htm

Basseville, M., A. Benveniste, M. Goursat, L. Hermans, L. Mevel and H. Van der Auweraer, 2001, "Output-Only Subspace-Based Identification: From Theory to Industrial Testing Practice", *Journal of Dynamic Systems, Measurement and Control, Transactions of the ASME*, Vol. 123, No. 4, pp. 668-676.

Bendat, J. S. and A. G. Piersol, 1980, *Engineering Applications of Correlation and Spectral Analysis*, Wiley-Interscience, New York.

Bernal, D., S. J. Dyke, J. L. Beck and H. F. Lam, 2002, "Phase II of the ASCE Benchmark Study on Structural Health Monitoring", *Proceedings of the 15th ASCE Engineering Mechanics Conference*, New York.

Ching, J. and J. L. Beck, 2003, "Two-Stage Bayesian Structural Health Monitoring Approach for Phase II ASCE Experimental Benchmark Studies", *Proceedings of the16th ASCE Engineering Mechanics Conference*, Seattle, Washington.

Dyke, S. J., D. Bernal, J. L. Beck and C. Ventura, 2003, "Experimental Phase of the Structural Health Monitoring Benchmark Problem", *Proceedings of the16th ASCE Engineering Mechanics Conference*, Seattle, Washington.

Ewins, D. J., 1995, *Modal Testing: Theory and Practice*, Research Studies Press, England.

Farrar, C. R. and S. W. Doebling, 1997, "An Overview of Modal-Based Damage Identification Methods", *Proceedings of the 1st International Conference on Damage Assessment of Structures (DAMAS)*, Sheffield, UK.

Franco, G., 2003, *Application of Evolutionary Strategies to Structural System Identification and Damage Detection*, Ph.D. Dissertation, Department of Civil Engineering, Columbia University, New York.

Goethals, I., B. Vanluyten and B. De Moor, 2004, "Reliable Spurious Mode Rejection Using Self Learning Algorithms", *Proceedings of the International Conference on Noise and Vibration Engineering (ISMA2004)*, Leuven, Belgium.

Guidorzi, R., 2003, *Multivariable System Identification*, Bononia University Press, Italy.

Guyader, A. and L. Mevel, 2003, "Covariance-Driven Subspace Methods: Input/Output vs. Output-Only", *Proceedings of the 21st International Modal Analysis Conference (IMAC-XXI)*, Kissimmee, Florida.

Ho, B. L. and R. E. Kalman, 1966, "Effective Construction of Linear State Variable Models for Input Output Functions", *Regelungstechnik*, Vol. 14, No. 12, pp. 545-548.

Ibrahim, S. R., 1977, "Random Decrement Technique for Modal Identification of Structures", *Journal of Spacecraft*, Vol. 14, No. 11, pp. 696-700.

James, G. H., T. G. Carne and J. P. Lauffer, 1993, *The Natural Excitation Technique for Modal Parameter Extraction from Operating Wind Turbines*, SAND92-1666, UC-261, Sandia National Laboratories.

Juang, J. N. and R. N. Pappa, 1985, "An Eigensystem Realization Algorithm for Modal Parameter Identification and Reduction", *Journal of Guidance, Control, and Dynamics*, Vol. 8, No. 5, pp. 620-627.

Juang, J. N., M. Phan, L. G. Horta and R. W. Longman, 1993, "Identification of Observer/Kalman Filter Markov Parameters: Theory and Experiments", *Journal of Guidance, Control, and Dynamics*, Vol. 16, No. 2, pp. 320-329.

Kailath, T., 1980, *Linear Systems*, Prentice Hall, New Jersey.

Ljung, L., 1999, *System Identification: Theory for the User*, 2nd Ed., Prentice Hall, New Jersey.

Luş, H., R. Betti and R. W. Longman, 1999, "Identification of Linear Structural Systems Using Earthquake-Induced Vibration Data", *Earthquake Engineering and Structural Dynamics*, Vol. 28, No. 11, pp. 1449-1467.

Luş, H., R. Betti and R. W. Longman, 2002, "Obtaining Refined First-Order Predictive Models of Linear Structural Systems", *Earthquake Engineering and Structural Dynamics*, Vol. 31, No. 7, pp. 1413-1440.

Luş, H., M. De Angelis, R. Betti and R. W. Longman, 2003, "Constructing Second-Order Models of Mechanical Systems from Identified State Space Realizations. Part I: Theoretical Discussions", *Journal of Engineering Mechanics*, Vol. 129, No. 5, pp. 477-488.

Luş, H., R. Betti and S. F. Masri, 2004, "Modeling of Long Span Bridges Using Vibration Measurements", Proceedings of the International Association of Bridge Management and Safety (IABMAS) Conference, Kyoto, Japan.

McKelvey, T., 1995, *Identification of State-Space Models from Time and Frequency Data*, Ph.D. Dissertation, Department of Electrical Engineering, Linköping University, Sweden.

Mottershead, J. E. and M. I. Friswell, 1993, "Model Updating in Structural Dynamics: A Survey", *Journal of Sound and Vibration*, Vol. 167, No. 2, pp. 347-375.

Pappa, R. S. and J. N. Juang, 1985, "Galileo Spacecraft Modal Identification Using an Eigensystem Realization Algorithm", *Journal of the Astronautical Sciences*, Vol. 33, No. 1, pp. 15-33.

Pappa, R. S., K. B. Elliott and A. Schenk, 1993, "Consistent-Mode Indicator for the Eigensystem Realization Algorithm", *Journal of Guidance, Control, and Dynamics*, Vol. 16, No. 5, pp. 852-858.

Peeters, B., J. Maeck and G. De Roeck, 2001a, "Vibration-Based Damage Detection in Civil Engineering: Excitation Sources and Temperature Effects", *Smart Materials and Structures*, Vol. 10, No. 3, pp. 518-527.

Peeters, B and G. De Roeck, 2001b, "Stochastic System Identification for Operational Modal Analysis: A Review", *Journal of Dynamic Systems, Measurement and Control, Transactions of the ASME*, Vol. 123, No. 4, pp. 659-667.

Peeters, B., 2000, *System identification and damage detection in civil engineering*, Ph.D. Dissertation, Department of Civil Engineering, K.U. Leuven, Belgium.

Pridham, B. A. and J. C. Wilson, 2002, "Subspace Identification of Vincent Thomas Suspension Bridge Ambient Vibration Data", *Proceedings of the 20th International Modal Analysis Conference (IMAC-XX)*, Los Angeles, California, pp.596-604.

Rytter, A., 1993, *Vibration Based Inspection of Civil Engineering Structures*, Ph.D. Dissertation, Department of Building Technology and Structural Engineering, Aolborg University, Denmark.

Shih, C. Y., Y. G. Tsuei, R. J. Allemang and D. L. Brown, 1988, "Complex Mode Indicator Function and Its Application to Spatial Domain Parameter Estimation", *Mechanical Systems and Signal Processing*, Vol. 2, No. 4, pp. 367-377.

Stoica, P. and R. Moses, 2005, *Spectral Analysis of Signals*, Prentice Hall, New Jersey.

Tolson, R. H., 1991, *Time Domain Modal Identification Methods for Application to Space Station Freedom Modal Identification Experiment*, NAS1-18458, Task No. 36, George Washington University.

Van der Auwaraer, H., 2001, "Structural Dynamics Modeling Using Modal Analysis: Applications, Trends and Challenges", *Proceedings of the 2001 IEEE Instrumentation and Measurement Technology Conference*, Budapest, Hungary, pp.1502-1509.

Van Overschee, P. and B. De Moor, 1993, "Subspace Algorithms for the Stochastic Identification Problem", *Automatica*, Vol. 29, No. 3, pp. 649-660.

Van Overschee, P. and B. De Moor, 1994, "N4SID: Subspace Algorithms for the Identification of Combined Deterministic-Stochastic Systems", *Automatica*, Vol. 30, No. 3, pp. 75-93.

Van Overschee, P. and B. De Moor, 1996, *Subspace Identification for Linear Systems: Theory-Implementation-Applications*, Kluwer Academic Publishers, Dordrecht, The Netherlands.

Viberg, M., 1995, "Subspace-Based Methods for the Identification of Linear Time-Invariant Systems", *Automatica*, Vol. 31, No. 12, pp.1835-1853.